INSTITUTE OF ASTRONOMY
UNIVERSITY OF AARHUS
DK-8000 AARHUS C
DENMARK

AARHUS - ASTRO - 1990 - 3

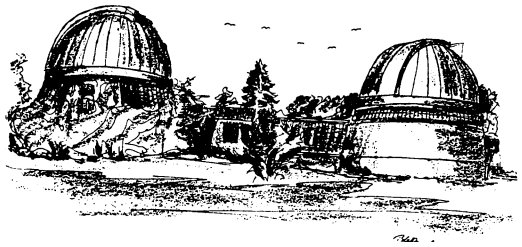

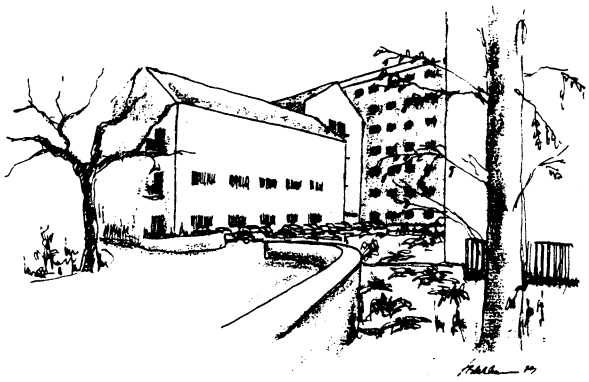

THE DEPTH OF THE SOLAR CONVECTION ZONE

J. Christensen-Dalsgaard, D.O. Gough and M.J. Thompson

Abstract

The transition of the temperature gradient between being subadiabatic and adiabatic at the base of the solar convection zone gives rise to a clear signature in the sound speed. Helioseismic measurements of the sound speed therefore permit a determination of the location of the base of the convection zone. We have tested two techniques by applying them to artificial data, obtained by adding simulated noise to frequencies computed from two different solar models. The determinations appear to be relatively insensitive to uncertainties of the physics of the solar interior, although, if present, a large-scale megagauss magnetic field at the base of the convection zone might have a significant effect on the results. On the assumption that this is not the case we conclude, from an analysis of observed frequencies of solar oscillation, that the depth of the solar convection zone is (0.287 ± 0.003) solar radii.

Submitted to **The Astrophysical Journal.**

THE DEPTH OF THE SOLAR CONVECTION ZONE

J. Christensen-Dalsgaard

Astronomisk Institut, Aarhus Universitet, Denmark; and

High Altitude Observatory, National Center for Atmospheric Research*

D. O. Gough

Institute of Astronomy, and Department of Applied Mathematics and Theoretical Physics,

University of Cambridge, England; and

Joint Institute for Laboratory Astrophysics, University of Colorado

M. J. Thompson

High Altitude Observatory, National Center for Atmospheric Research*

Received: _____

* The National Center for Atmospheric Research is sponsored by the National Science Foundation.

ABSTRACT

The transition of the temperature gradient between being subadiabatic and adiabatic at the base of the solar convection zone gives rise to a clear signature in the sound speed. Helioseismic measurements of the sound speed therefore permit a determination of the location of the base of the convection zone. We have tested two techniques by applying them to artificial data, obtained by adding simulated noise to frequencies computed from two different solar models. The determinations appear to be relatively insensitive to uncertainties of the physics of the solar interior, although, if present, a large-scale megagauss magnetic field at the base of the convection zone might have a significant effect on the results. On the assumption that this is not the case we conclude, from an analysis of observed frequencies of solar oscillation, that the depth of the solar convection zone is (0.287 ± 0.003) solar radii.

Subject headings: Sun: interior — Sun: oscillations — Sun: convection zone depth — helioseismology — Sun: lithium depletion

I. INTRODUCTION

The properties of the Sun's convection zone play a major role in many aspects of solar physics. In particular, it is presumed that the abundance of lithium in the convection zone, and consequently in the photosphere, has been depleted by nuclear transmutations to the observed photospheric level, which is considerably below the general cosmic value and the abundance in meteorites (e.g. Boesgaard and Steigman 1985; Anders and Grevesse 1989). The fact that lithium has not been completely destroyed indicates that vigorous mixing cannot extend to regions where the temperature is greater than about 2.5×10^6 K, because at such temperatures the lithium destruction time scale is comparable with or shorter than the age of the Sun. On the other hand, beryllium, for which substantial destruction takes place only at temperatures exceeding 3.4×10^6 K, appears to have been at most slightly depleted (Anders and Grevesse 1989). It is evident that the rate of lithium and beryllium destruction, and hence the expected solar photospheric abundances, must depend strongly on the temperature at the base of the convection zone. Another issue is atomic diffusion, which could have a significant effect on the chemical composition of the solar material within and beneath the convection zone (e.g. Noerdlinger 1977; Gabriel, Noels and Scuflaire 1984; Wambsganss 1988; Cox, Guzik and Kidman 1989); this affects not only the observed surface abundances but also the overall structure of the Sun. The diffusion time scale is a sensitive function of conditions at the point where macroscopic mixing ceases to be effective.

There are several other issues upon which the extent of the convection zone bears. For example, it is widely believed that the solar magnetic activity originates through some form of dynamo process, taking place either in the convection zone (see, for example, the review by Parker 1987) or in a thin layer at its base (Parker 1975; also, for example, DeLuca and Gilman 1986 and references therein). Numerical simulations (e.g. Gilman and Miller 1986) have revealed that the depth of the convection zone has an important controlling effect on the form of the differential rotation. Through the differential rotation, the depth is therefore likely to affect the details of the dynamo process and

the surface manifestation of magnetic activity. Thus it is evidently of considerable importance to determine the radius, and other properties, at the base of the convection zone.

Conditions near the base of the convection zone are uncertain. In most computations of solar models it is assumed that motion extends only over the region where the star is convectively unstable according to the Schwarzschild criterion, namely where

$$\gamma^{-1} - \frac{d\ln\rho}{d\ln p} > 0. \tag{1.1}$$

Here $\gamma = (\partial \ln p/\partial \ln \rho)_s$, p being pressure and ρ density, the partial derivative being taken at constant specific entropy s, and $d\ln\rho/d\ln p$ characterizes the actual stratification of the equilibrium state. In a region of uniform chemical composition the criterion (1.1) can be rewritten in terms of gradients of temperature T as

$$\nabla > \nabla_{ad}, \tag{1.2}$$

where $\nabla_{ad} = (\partial \ln T/\partial \ln p)_s$ and $\nabla \equiv d\ln T/d\ln p$. This is the form of the instability condition that is most commonly used in astrophysics. In the convection zone the value of ∇ is determined by the condition that the luminosity can be carried by radiation and convection together, the latter being described by some form of mixing-length theory. In practice, however, the heat content of matter near the base of the convection zone is so great that only a very small superadiabatic gradient $\nabla - \nabla_{ad}$ suffices for transporting the luminosity by convection. Thus in the deeper parts of the convection zone the condition $\nabla = \nabla_{ad}$ is satisfied quite accurately (e.g. Gough and Weiss 1976). This has been confirmed by helioseismic inversion (Gough 1984). Beneath the convection zone, energy is generally assumed to be transported by radiation alone, and $\nabla = \nabla_{rad}$, where ∇_{rad} is the value of ∇ that would be required to transport the entire solar luminosity by radiation.

In reality it is evident that convective motion does not stop immediately where the instability condition (1.2) ceases to be satisfied. There is a region of overshoot, into which the convective motion penetrates before being deflected by pressure fluctuations associated with the opposing buoyancy

forces. The extent of the overshoot region, and the dynamics within it, are currently quite uncertain. Throughout much of it motion is no doubt sufficiently rapid to maintain the temperature gradient essentially at the adiabatic value. Furthermore, energy transport by low-frequency gravity waves, which are likely to be generated in this region, may also modify the temperature distribution. At the base of the overshoot region there must be a transition, which could be quite abrupt, to the radiative gradient in the region beneath where the motion is too feeble to transport much heat.

In the present paper we are not explicitly concerned with the nature of the transition. Thus, when we discuss the extent of the convection zone we are referring to the extent of the essentially adiabatically stratified region; it must be kept in mind that in reality this includes the adiabatic part of the overshoot region. Since this region is also mixed on a short time scale, the distinction between the simplified description without and the realistic description with overshooting is unlikely to be important for the analysis of lithium destruction and material diffusion, although it might be significant for the possible generation of magnetic field beneath the convection zone.

Inferences about the depth d_b of the convection zone on the basis of observed frequencies of solar oscillation were made very early in the development of helioseismology. From Deubner's (1975) observations, and using a simplified description of the oscillations, Gough (1977) concluded that the actual solar convection zone was deeper by about 50 per cent than that in the model of Ando and Osaki (1975), implying a depth of about $0.3R$, where R is the radius of the Sun. From similar observations, and using the numerical computations of Ulrich and Rhodes (1977), Rhodes, Ulrich and Simon (1977) were able to estimate a lower limit of $0.25R$ on the convection zone depth. Studies of the sensitivity of oscillation frequencies to uncertainties in the physics of the convection zone were subsequently carried out by Lubow, Rhodes and Ulrich (1980) and by Berthomieu *et al.* (1980), the latter concluding that $d_b \simeq 200$ Mm $\simeq 0.3R$. In all these cases, however, only high-degree modes were analyzed. These are trapped in just the outer few per cent of the solar convection zone, and hence carry no direct information about its depth. Instead, the observed frequencies effectively

allowed a determination of the adiabat in the adiabatic part of the convection zone, and the depth of the convection zone was obtained through computation of envelope models along this adiabat. Thus a considerable amount of theoretical extrapolation was involved in estimating d_b.

Gough (1986) pointed out that a much more direct determination of the convection-zone depth can be obtained by considering the gradient in the sound speed, as obtained by inversion of observed frequencies of solar oscillations (e.g. Christensen-Dalsgaard *et al.* 1985; Brodsky and Vorontsov 1987; Christensen-Dalsgaard, Gough and Thompson 1988; Kosovichev 1988; Shibahashi and Sekii 1988). The sound-speed gradient is closely related to the temperature gradient; thus the transition from an adiabatic temperature gradient within the convection zone to a subadiabatic gradient beneath it is visible as a clear break in the gradient of the sound speed. This was evident in the first inversion of p-mode data that extended into the radiative interior (Christensen-Dalsgaard *et al.* 1985). The inferred sound speed is reproduced here in Figure 1, in which a transition at a radius r between $0.71R$ and $0.72R$ is quite apparent (see the inset to the figure).

The transition is more prominent in a plot of the sound-speed gradient itself. In the lower convection zone the sound-speed squared is given approximately by

$$c^2 \simeq (\gamma - 1)\frac{GM}{R}\left(\frac{R}{r} - 1\right) \tag{1.3}$$

(Christensen-Dalsgaard 1986; see § IV and Appendix A); here M is the solar mass and G is the gravitational constant. Thus the quantity

$$W = \frac{r^2}{GM}\frac{dc^2}{dr} \tag{1.4}$$

is approximately constant deep in the convection zone, and takes the value $-2/3$ for $\gamma = 5/3$. Beneath the convection zone W increases abruptly (see § IV). By locating this transition, Gough (1986) deduced the values of d_b in several unknown solar models with an uncertainty of about $0.01R$. Vorontsov (1988) used essentially the same method (but with a somewhat different inversion technique to infer c) on solar frequencies, estimating the radius r_b of the base of the convection

zone to be $0.70 \pm 0.01R$. Further discussion of the technique has been presented by Vorontsov and Zharkov (1989).

In this paper we report further results of using this technique. The sound speed has been inferred by different asymptotic approaches from the observed frequencies presented by Duvall *et al.* (1988) and Libbrecht and Kaufman (1988). One approach is *absolute*, in the sense that the sound speed is obtained directly from the frequencies, without the use of solar models. In the second approach, a *differential* inversion is carried out for the sound-speed difference between the Sun and one or more reference models. To test the sensitivity of the inferences to systematic or random errors in the observed data, or systematic errors in the inversion procedures, we have carried out a set of analyses on artificial data. One of us (A) computed solar models and frequencies for these models of the modes in the observed data set. He also added errors, both random and systematic, to the frequencies. Some care was taken to include at least one realization of errors whose statistical properties were similar to the estimated errors of the observed data. These data were then analyzed by the other two authors (B and C) using different techniques. The analysis was initially carried out in a "blind" fashion, the frequencies being the only information provided about the unknown models. For each model several realizations of the errors were considered, starting with the largest errors. Further data were provided only after the analysis of the previous set had been completed, and the results had been reported to author A. Finally the computed frequencies, without errors, were analyzed. We subsequently carried out additional more detailed analyses, in an attempt to understand the results obtained from the initial sets of inversions. On this basis we are able to estimate the likely uncertainty in the determination d_b from the observed solar frequencies.

One potential uncertainty which we have ignored might result from a large-scale magnetic field beneath the base of the convection zone. It is conceivable that such a field could change the propagation properties of the modes in this region in such a way as to mimic an extension of the adiabatically stratified region, and hence lead us to infer an excessive depth of the convection zone.

In § VIII we present a crude estimate of the magnitude of this effect, which suggests that a field of the order of a megagauss might cause an error of of the order of $0.01R$ in the inferred d_b. However, we emphasize that a more careful analysis would be required to obtain reliable estimates of the likely effects of realistic field configurations. Such an analysis is beyond the scope of the present paper.

The contents of the remainder of the paper are as follows. In § II we sketch the theoretical basis for the two sound-speed inversion techniques we have employed. The solar models used for producing artificial data to test our inversion procedures are described in § III, together with details of the random and systematic errors that were added to the test data. The results of the tests of the absolute and differential methods are presented in §§ IV and V respectively, and the results from real solar data are described in § VI. Inferences regarding the temperature at the base of the Sun's convection zone are presented in § VII. In § VIII we discuss our findings, which are briefly summarized in § IX.

II. THE SOUND-SPEED INVERSION

a) The absolute method

The absolute method is essentially as described by Gough (1986), and utilizes the Duvall relation

$$\frac{[n+\alpha(\omega)]\pi}{\omega} \simeq F(w) \equiv \int_{\ln r_t}^{\ln R} \left(1-\frac{a^2}{w^2}\right)^{\frac{1}{2}} a^{-1} d\ln r. \qquad (2.1)$$

Here ω is the angular frequency of a mode of order n and degree l, $w = \omega/L$ where $L = l + \frac{1}{2}$, $a = c/r$ and r_t is the radius at which $a = w$. Since ω and (indirectly) n can be determined from observation, $F(w)$ can be obtained by choosing α to make the left-hand side of equation (2.1) as nearly as possible a function only of w. The phase $\alpha(\omega)$ depends principally on conditions in the

surface layers of the star; it can be determined from the observations only to within a multiple of ω. By differentiating equation (2.1) with respect to w one obtains

$$w^3 \frac{dF}{dw} = \int_{\ln r_t}^{\ln R} \left(a^{-2} - w^{-2}\right)^{-\frac{1}{2}} d\ln r. \tag{2.2}$$

(Note that this equation is unaffected by the fact that α has been determined only to within a multiple of ω, and $F(w)$ only to within a constant.) Equation (2.2) is of the Abel type and can therefore be inverted to obtain c as a function of r. From this W can be computed trivially.

The procedure for determining the function F was outlined by Gough (1986), and is presented in Appendix B. Only modes of radial order $n \geq 2$ were included in the analysis.

b) The differential method.

By perturbing equation (2.1) and linearizing in small quantities one can obtain an approximate relation between the frequencies of oscillation of the Sun and those of some known reference model and their internal sound speeds:

$$\left(S(w) - \pi \frac{d\alpha}{d\omega}\right) \frac{\delta\omega}{\omega} = \int_{\ln r_t}^{\ln R} \left(1 - \frac{a^2}{w^2}\right)^{-\frac{1}{2}} \frac{\delta c}{c} a^{-1} d\ln r + \pi \frac{\delta\alpha(\omega)}{\omega}, \tag{2.3}$$

where $\delta\omega$, δc and $\delta\alpha$ are the differences in frequency, sound speed (at constant r) and phase (at constant ω) between the Sun and the reference model,

$$S(w) = \int_{\ln r_t}^{\ln R} \left(1 - \frac{a^2}{w^2}\right)^{-\frac{1}{2}} a^{-1} d\ln r, \tag{2.4}$$

and all unperturbed quantities are evaluated for the known model. On the left-hand side of equation (2.3) $\delta\omega/\omega$ can be obtained from observation, and the bracket is determined from the reference model. The first term on the right-hand side of this equation depends on ω and l in the combination $w \equiv \omega/L$, while the second term is a function of ω, so that equation (2.3) can be rewritten

$$\left(S(w) - \pi \frac{d\alpha}{d\omega}\right) \frac{\delta\omega}{\omega} = H_1(w) + H_2(\omega). \tag{2.5}$$

Because H_1 and H_2 depend only on w and ω respectively, they can be separated in the data. This is achieved by making a least-squares fit of a function $\overline{H}_1(w) + \overline{H}_2(\omega)$ to the scaled data, where $\overline{H}_1$ and $\overline{H}_2$ are cubic splines. The H_1 term leads to an integral equation of the Abel type which can be inverted to obtain $\delta c/c$ and hence the sound speed in the solar interior. Once again, W can thence be calculated, by substituting $c^2(1 + 2\delta c/c)$ for c^2 into equation (1.4).

The details of the inversion method are given by Christensen-Dalsgaard, Gough and Thompson (1989). The distribution of spline knots for the fitted functions $\overline{H}_1$ and $\overline{H}_2$ was chosen to be the same as in that paper: in brief, knots uniformly spaced in ω and in $\log w$ (except at large w). In all cases 20 knots in ω were used, while the number of w-knots varied between 20 and 36. Some low-frequency, low-degree modes, for which equation (2.1) is not well satisfied, were excluded from the inversions, as specified by Christensen-Dalsgaard, Gough and Thompson (1988). Also, of course, the f modes ($n = 0$) were excluded; but the $n = 1$ modes were retained.

III. THE OBSERVED AND THE ARTIFICIAL DATA

The sound-speed inversions were based on observed frequencies listed by Duvall *et al.* (1988), which comprise modes with degree $l \leq 99$, and those of Libbrecht and Kaufman (1988). It was noted by Christensen-Dalsgaard, Gough and Thompson (1988; see also § VI*b* below) that there appears to be a systematic difference between the two sets. For this reason we have preferred to use only those modes given by Libbrecht and Kaufman with $l \geq 100$. The resulting mode set contained 1632 p modes.

To test the inversion procedures, they were applied to artificial data, spanning the same set of modes as the observed data. In computing the data, the principal goal was to test the sensitivity of the determination of the convection zone depth to other probable uncertainties in the properties of the Sun, and to errors in the data. In particular, the properties of the solar core, or of low-degree modes, are not immediately relevant. Nevertheless, it was of interest to use these data also as a

contribution to the more general evaluation of inversion techniques. Thus the data include features that are not directly relevant to the determination of the depth of the convection zone, and the "observers" (authors B and C) made some attempts to extract such features.

Two unknown models, Model X and Model Y, were considered. Both models used the Eggleton, Faulkner and Flannery (1973) equation of state. To add flexibility to the definition of the models, it was desirable to be able to control the depth of the convection zone; this was accomplished by modifying artificially the opacity in the temperature range corresponding to the region near its base. Specifically, the opacity κ, as a function of density ρ and temperature T, was determined from

$$\log \kappa = \log \kappa_0 + A\psi(\log T). \tag{3.1}$$

Here κ_0 was obtained from interpolation in either the Cox and Tabor (1976; CT) tables or in tables based on the Los Alamos Opacity Library (Huebner *et al.* 1977; LAOL). The function ψ is defined by $\psi(x) = \exp[-(y/\Delta \log T)^2]$, where

$$y = \begin{cases} x - \log T_1 & \text{for } x < \log T_1 \\ 0 & \text{for } \log T_1 < x < \log T_2 \\ x - \log T_2 & \text{for } \log T_2 < x. \end{cases} \tag{3.2}$$

This definition provides an opacity modification over a well-defined region in $\log T$, with a continuous transition to zero on either side. The nuclear reaction rates were essentially as presented by Parker (1986) and Bahcall and Ulrich (1988). The hydrogen abundance profile $X(q)$ was obtained by scaling a reference profile $X_r(q)$ by a constant factor; the factor, and the mixing length parameter, were chosen to get a model having the solar radius and a prescribed luminosity. The computation used 600 spatial mesh points. The model computation was otherwise as described by Christensen-Dalsgaard (1982).

In Model X the opacity increase was quite large, and covered a substantial fraction of the radiative interior. As a result a relatively large helium abundance was required to match the assumed luminosity. The reference hydrogen profile was taken from a normal evolved solar model. The

opacity modification for Model Y was modest, and the surface helium abundance was closer to normal. Here, however, the $X_r(q)$ was intermediate between a normal model and the diffusively mixed model, having a so-called turbulent Reynolds number Re^* of 100, of Schatzman *et al.* (1981).

The most important distinctive properties of the models are summarized in Table 1.

Adiabatic oscillation frequencies were computed for the models, after they had been transferred to a mesh suitable for resolving the structure of the p-mode eigenfunctions. The calculation used 1200 mesh points. This ensures that the internal precision in the frequency calculation is better than 0.1 μHz. To the computed frequencies were added random errors which were modelled on the basis of a parametrized fit to the standard deviations quoted by Duvall *et al.* (1988) and Libbrecht and Kaufman (1988). Specifically the random component of the frequency error was determined as random numbers with an approximately Gaussian distribution, with standard deviation $\sigma(\nu)$ determined by

$$\sigma(\nu)^2 = \sigma_w^2 + \sigma_\nu^2. \tag{3.3}$$

Here

$$\sigma_w^2 = A_w^2 \left[\left(\frac{w^*}{w} \right)^3 + 1 \right], \qquad \sigma_\nu^2 = A_\nu^2 \left(\frac{\nu}{\nu_{max}} \right)^5. \tag{3.4}$$

For $A_w = 0.2\mu$Hz, $A_\nu = 3\mu$Hz, $w^*/2\pi = 120\mu$Hz and $\nu_{max} = 5000\mu$Hz the resulting standard deviation is similar to that of the observed data.

To simulate the systematic error mentioned above, for Model X we also considered a case where, in addition to these random errors, a scale error of 0.5 per cent in linear scale was added to the modes of degree greater than 120. This was implemented by subtracting from each such frequency a relative change of 0.25 per cent. Figure 2 shows the resulting errors in this case. In the remaining cases, no systematic errors were included. The parameters characterizing the random errors were varied, to get an indication of the sensitivity of the inversion to the error properties of the data. These parameters are given in Table 2. Different realizations of the random numbers were used in each case.

IV. TEST OF THE ABSOLUTE INVERSION METHOD

As discussed in § I, the function $W(r)$ defined by equation (1.4) can be used as a accurate indicator of the position of the base of the convection zone. The intersection with $-2/3$ of a simple linear extrapolation from the steeply descending part of the graph of $W(r)$ gives a very reasonable estimate of the depth of the convection zone: by this means Gough (1986) obtained the depths of the convection zones of three unknown models to better than $0.005R$. In the present paper we use a slightly more sophisticated technique which can be automated with greater rigour. Approximate analytic expressions are derived for the square of the sound speed just beneath and above the base of the convection zones. To a first approximation the expression in the convective region has no free parameters, while the expression in the radiative region has several, one of which (implicitly) is the radius r_b at which the base of the convection zone is located. Two constraints on the free parameters are obtained by requiring continuity of c^2 and W at r_b. The remaining free parameters are then estimated by making a least-squares fit of the analytic expression to the sound-speed squared inferred from observational data. This is done over a region of the radiative interior that is beneath the convection zone and yet sufficiently close that the analytic approximations are still reasonable. Hence an estimate of r_b is obtained.

The lower part of the convection zone is very close to being adiabatically stratified. Moreover, the adiabatic exponent γ is almost constant (and approximately equal to 5/3). Hence

$$p \propto \rho^\gamma. \tag{4.1}$$

This determines the functional form of the sound speed $c(r)$. In this region the heat capacity of the fluid is high, and therefore the characteristic Mach number of the convective motion responsible for the transport is very low. Consequently the hydrostatic equation:

$$\frac{dp}{dr} = -\frac{Gm\rho}{r^2}, \tag{4.2}$$

where m is the mass contained within the sphere concentric with the Sun of radius r, is satisfied quite accurately. Moreover, the mass of the convection zone is small (about $0.02M$), so m is approximately constant. As shown in Appendix A, an approximate expression for c^2 may be derived from equations (4.1) and (4.2) (cf. equation A9). If the variation of m through the convection zone is neglected, this expression essentially reduces to equation (1.3) discussed previously.

In the outer layers of the radiative interior immediately beneath the convection zone it is still a good approximation to ignore the variation of m when integrating equation (4.2). Here, the temperature stratification is determined by the radiative transfer relation so that

$$\frac{dT}{dr} \propto -\frac{\kappa\rho}{r^2T^3}, \tag{4.3}$$

where κ is opacity which we approximate by $\kappa \propto \rho^\lambda T^{-\nu}$, λ and ν being constants. Relation (4.2) divided by relation (4.3) yields an expression for dp/dT. Furthermore, ρ can be eliminated with the help of the perfect gas law

$$p = \frac{\mathcal{R}\rho T}{\mu}, \tag{4.4}$$

where $\mathcal{R}$ is the gas constant per mole ($\mathcal{R} = k_B/m_u$ where k_B is Boltzmann's constant and m_u is the atomic mass unit); here μ is the mean molecular weight, which is nearly constant because hydrogen and helium are essentially fully ionized. Then the expression for dp/dT can be integrated, resulting in

$$p^{\lambda+1} \propto T^{\lambda+\nu+4} + T_0^{\lambda+\nu+4}, \tag{4.5}$$

where T_0 is a constant of integration. Provided $T_0 \ll T$, which must be confirmed *a posteriori*, the relation between p and ρ determined by equations (4.3) and (4.5) can be expanded about $T_0/T = 0$. The expansion can be used to close the hydrostatic relation (4.1), which can then be integrated to give the sound speed in the form

$$c^2 \simeq \gamma(1-\Gamma^{-1})\frac{GM}{R}\xi f(\xi), \tag{4.6}$$

where

$$\Gamma = \frac{a}{\nu + 3}, \tag{4.7}$$

$$a = \lambda + \nu + 4, \tag{4.8}$$

and the dimensionless independent variable ξ is given by

$$\xi(r) = \frac{R}{r} - \frac{R}{r_0}, \tag{4.9}$$

where r_0 is another constant of integration. The function f is given by

$$f(\xi) = 1 - \delta\xi^{-a} - A\delta^2\xi^{-2a} - \cdots; \tag{4.10}$$

here the constant δ is proportional to T_0^a, and is therefore yet undetermined, and the quantity A is a somewhat cumbersome combination, of order unity, of the exponents λ and ν: the details are given in Appendix A.

Because the exponent a is quite large ($a = 8.5$ for Kramers' law) the function f rapidly approaches unity as r decreases. Thus there is a thin transition layer immediately beneath the convection zone, below which the functional form of c^2 given by equation (4.6) becomes similar to that given by equation (1.3). The principal difference between the two expressions is then the value of the sound-speed gradient, for which we use the measure W defined by equation (1.4). Thus we obtain

$$W \simeq -\gamma(1 - \gamma^{-1}) \simeq -0.67 \tag{4.11}$$

in the convection zone, and

$$W \simeq -\gamma(1 - \Gamma^{-1})\left(1 + \xi\frac{df}{d\xi}\right) \tag{4.12}$$

immediately beneath the convection zone where it is still valid to ignore the derivative of m. Beneath the transition layer $df/d\ln\xi$ is small, and if the variation in m could still be ignored W would approach a constant, which takes the value -0.39 for Kramers' opacity. It is because the transition

between the two constant values of W is quite abrupt that the extent of the convection zone can be seen quite clearly even in a plot of c^2 against r.

Because p and T must be continuous, ρ is continuous, and therefore so is the sound speed. This deduction depends on assuming the chemical composition to be continuous; indeed, it is normally considered to be essentially uniform outside the energy-generating core. Moreover, if convective overshooting is ignored, the base of the convection zone is determined by the condition $d\ln\rho/d\ln p = \gamma^{-1}$. Therefore $d\ln\rho/d\ln p$ is continuous, and since via the equation of hydrostatic support continuity of ρ implies that the pressure gradient is continuous, it follows that the gradient of the sound speed is also continuous. The integration constants δ and A in equation (4.10) can thus be expressed in terms of r_b by demanding continuity of c^2 and W at the base $r = r_b$ of the convection zone. The formulae are recorded in Appendix A. We simply point out here that if, for example, the Kramers exponents $\lambda = 1$, $\nu = 3.5$ are adopted and $r_b = 0.71R$, then $\delta\xi_b^{-a} = 0.077$, where $\xi_b = \xi(r_b)$, confirming that f does not differ substantially from unity.

In the radiative region beneath the convection zone, between suitably chosen radii r_1 and r_2, a least-squares fit of the approximation (4.6) – (4.10) was made to the square of the sound speed inferred from the inversion of the frequencies. Continuity with the expression (1.3) for c^2 in the convection zone, and continuity of W given by equations (4.11) and (4.12), were assumed, in the manner described in Appendix A. Thus formally the minimization is over three parameters, which can be taken to be λ, ν and ξ_b. In fact we assumed $\lambda = 1$, which is valid for Kramer's opacity law, and performed the regression over ν and ξ_b only. (The fit with three free parameters was found to produce too flat a minimum for the solution to be reliable.) In all cases we took $r_1 = 0.5R$ and $r_2 = 0.67R$.

This procedure has been applied to the data sets described in § III. The results, which were obtained by author B with no prior knowledge of the unknown models except for their p-mode frequencies, are shown in Table 3. The accuracy of the inferences for Model X is very encouraging:

for the error-free data set the error in the inferred depth is less than $0.001R$, while for the sets with the largest errors the inferred depth is still accurate to better than $0.01R$. The results for Model Y are also accurate to better than $0.01R$, except curiously for data set Y.0 (the error-free case) for which the error in the inferred depth is $1.05 \times 10^{-2}R$.

It may be noted that the inferred values of ν, which are also given in Table 3, are rather high. Assuming a smaller value for λ would reduce the value of ν, bringing the opacity exponents closer to theory. However, in our experience this can make the inferred depth of the convection zone less accurate: for example, if one takes $\lambda = 0.75$ for data set X.0, the inferred values of ν and d_b are 4.4 and $0.735R$ respectively. It is possible that the high values of ν in fact result from an inaccuracy in the analytic approximation: in particular it may be that the variation of m cannot be ignored at radii as small as $0.5R$. Nonetheless, the accuracy of the depths inferred in these blind experiments is reasonable. If the errors included in the artificial data are representative of those in real solar data, we estimate that the standard error in the depth determination for the solar convection zone (§ VI) using the absolute method is $\pm 0.01R$.

V. TEST OF THE DIFFERENTIAL INVERSION METHOD.

a) Reference models

The differential inversion method is capable of inferring the run of sound speed with considerable accuracy; in tests with artificial data it has proved possible to recover the sound speed over a wide range of depths with an error much less than one per cent (Christensen-Dalsgaard, Gough and Thompson 1989). However, an obvious potential drawback is that the results might depend on the details of the reference model that is being used. Thus we have to investigate the sensitivity of the results to the physics of the reference model. Furthermore, because of the rapid change in the sound-speed gradient beneath the convection zone, the sound-speed difference between two

models with convection zones of different depths exhibits a sharp feature in the region that is adiabatically stratified on one model but not the other. Such a feature is badly resolved by the inversion (Christensen-Dalsgaard *et al.* 1989; see also § V*b* below) and may therefore cause problems for the evaluation of W. For this reason it is desirable to use reference models with as nearly as possible the correct depth of the convection zone. Hence we have used a fairly extensive set of models, with different assumptions about the input physics, and with varying depths of convection zone. All models were calibrated to have solar radius and luminosity. The properties of the models are summarized in Table 4.

The set includes models at solar age from four complete evolution sequences, with differing equation of state or opacity. Furthermore, to obtain models spanning a range of different depths of convection zone, two sequences of static models were considered, the opacity being modified in the manner described by equation (3.1). The hydrogen abundance $X(q)$ was obtained from the abundance profile in an evolutionary model with the same basic physics, without modification to the opacity, by scaling with a constant factor. These sequences were based on the so-called MHD equation of state (cf. Hummer and Mihalas 1988; Mihalas, Däppen and Hummer 1988; Däppen *et al.* 1988); in one case the CT opacities were used, whereas the second sequence used the LAOL opacity tables.

The computation of the models and their adiabatic oscillation frequencies otherwise proceeded as in the case of the unknown models (cf. § III).

A striking feature of the results in Table 4 is the difference in envelope helium abundance Y_0 between models using the CT and models using the LAOL opacities. This is caused by the substantially higher opacities in the solar core in the LAOL case; in contrast, the artificial modification of the opacity near the base of the convection zone has a modest effect on Y_0.

b) Tests of the differential method

To determine the position of the base of the convection zone using the methods of this paper requires that the gradient of the sound speed be accurately inferred in that region. But, as has already been stated, when the convection zone in the reference model does not have the same depth as that in the unknown model (or the Sun), $\delta c/c$ exhibits a sharp feature which may be poorly resolved in the differential inversion; this in turn means that the inferred gradient dc/dr may be inaccurate there.

The result of the inversion for the relative sound-speed difference $\delta c/c$ would be imprecise even with error-free data, because of the limited resolution attainable with any given mode set. The resolution can be understood in terms of *averaging kernels* $\mathcal{K}(r, r_0)$ (Christensen-Dalsgaard, Schou and Thompson 1990). The inferred sound speed (denoted with an overbar) at any radius r_0 is in fact a weighted mean of the exact sound-speed difference at all radii:

$$\overline{\frac{\delta c}{c}}(r_0) = \int_0^R \mathcal{K}(r, r_0) \frac{\delta c}{c}(r) dr. \tag{5.1}$$

Equation (5.1) is actually not exact, because the frequency differences depend not only on $\delta c/c$ but also on the relative density differences, for example (see Gough and Thompson 1990 for more details); however, for five-minute p modes it is a very reasonable approximation. Asymptotic theory indicates that the averaging kernels in equation (5.1) have similar properties to those displayed for asymptotic rotational inversions by Christensen-Dalsgaard, Schou and Thompson, though they differ in detail.

We may in fact obtain a reasonable impression of the effect of limited resolution on the determination of the depth of the convection zone by the following crude model: namely, supposing that the inferred $\delta c/c$ is simply a running mean (with a certain characteristic width) of the exact $\delta c/c$. To be specific, we model the averaging kernels simply as truncated cosines:

$$\mathcal{K}(r, r_0) \propto \begin{cases} \cos \dfrac{\pi(r - r_0)}{3d} & \text{if } |r - r_0| < \frac{3}{2}d \\ 0 & \text{otherwise} \end{cases} \tag{5.2}$$

with normalization

$$\int_0^R \mathcal{K}(r, r_0) dr = 1. \tag{5.3}$$

Except near $r_0 = 0$ and $r_0 = R$, d is precisely the width measure of $\mathcal{K}$ adopted by Christensen-Dalsgaard *et al.*, i.e. the distance between the two quartile points. Typically, for inversions of current p-mode data sets, d is five to ten per cent of the solar radius near the base of the convection zone.

Figure 3a illustrates the case when an unknown model (in this case Model X of Table 1), which takes the role of the Sun, has a shallower convection zone than the reference model used (here model 10 of Table 4). The depths of the convection zones in these two models differ by $0.03R$. The exact $\delta c/c$ shows an abrupt step at the base of the shallower convection zone, but in the "inferred" sound-speed difference, which we obtained from the exact difference by artificially smoothing with $d = 0.07R$, the step is to some extent smoothed out. Figure 3b shows that the effect on the "inferred" function W is quite drastic. These effects are indeed rather similar to what is observed when an actual inversion is performed (Figures 5a and 5b, discussed below).

It might also be remarked in passing that Figure 3a illustrates very clearly that equation (1.3) holds only approximately, and that in the region where both models are adiabatically stratified $\delta c/c$ can deviate from zero. The deviation in $r \gtrsim 0.72R$ in the present case arises principally from the two models using different equations of state and hence having different adiabatic exponents where elements are partially ionized. The sound-speed difference is actually quite large in the ionization zones of the abundant elements, hydrogen and helium, and this affects even the deepest parts of the convection zone (see Christensen-Dalsgaard 1988); in addition, smaller-scale deviations, which clearly have an effect on W (Figure 3b), arise from differences in the adiabatic exponents in the ionization zones of heavier elements.

The case when the convection zones in the reference and unknown models are of roughly equal depth is shown in Figures 3c – 3d. The depths of the convection zones in the two models (Model X and reference model 6) differ by only $7 \times 10^{-4}R$. The smooth increase in $\delta c/c$ below $r \simeq 0.71R$

comes from the different opacities in the two models which affect the radiative interior. In Figures 3e and 3f the convection zone in the reference model (model 5 of Table 4) is shallower than that in Model X, but by a modest $4 \times 10^{-3}R$. This gives rise to a sharp corner in $\delta c/c$ at the base of the shallower convection zone, but the substantial increase in sound-speed difference at greater depth is once again caused by the difference in the physics of the radiative interior of the two models. The corner is not apparent in the artificially smoothed $\delta c/c$. In these two cases also, the effects of artificially smoothing according to equations (5.1) and (5.2) are similar to what is found in actual inversions (Figures 5c - 5f).

Figure 3 shows that in general, because of the smoothing due to imperfect resolution, the inferred function W depends on the reference model that is used and may be a rather poor estimate of the true W. To circumvent this problem, sound-speed inversions can be performed using a number of reference models with different convection zone depths. From the result of each inversion, an average deviation between the inferred W (W^{inf}) and W for the reference model (W^{ref}) is calculated:

$$\overline{\delta W} = (2\Delta)^{-1} \int_{r_b-\Delta}^{r_b+\Delta} [W^{inf}(r) - W^{ref}(r)]dr. \qquad (5.4)$$

Here r_b is the location of the base of the convection zone in the reference model, and Δ is some chosen (fixed) half-width over which the average is taken. Figures 3b and 3f suggest that if Δ is a few per cent of the solar radius the "inferred" $\overline{\delta W}$ is positive when the reference model's convection zone is rather shallower than that of the unknown model, and negative when it is somewhat deeper; that is, for these cases the sign of $\overline{\delta W}$ is the same as it would be if the inferred $\delta c/c$ were exact. When the convection zones in the unknown and reference models have almost the same depth, the inferred $\overline{\delta W}$ is close to zero. Thus the idea is to obtain a null result by finding for what depth of convection zone in the reference model the average deviation $\overline{\delta W}$ is zero. We have performed numerical experiments which verify that this determination is accurate and largely independent of other aspects of the reference models employed, using the reference models described in § Va.

Before discussing the tests performed using actual inversions, we continue to consider the effect of artificial smoothing as specified by equations (5.1 - 5.2). For this purpose we shall consider Model X (see § III) as the unknown model and use a subset of four of the reference models described above (models 5 - 8 in Table 4); the depths of their convection zones range from $0.267R$ to $0.283R$, while the depth of the convection zone in Model X is $0.271R$.

Figure 4 shows $\overline{\delta W}$ plotted against depth of convection zone computed for artificially smoothed relative sound-speed differences between Model X and the four reference models; here $\Delta = 0.02R$. The results for smoothing width $d = 0.07R$ are indicated with plus signs. By interpolating linearly among these points one would infer that $\overline{\delta W} = 0$ at a depth of $0.277R$. The error in this estimate of the depth of the convection zone of Model X is thus $6 \times 10^{-3}R$. This error arises principally from the sensitivity of the "inferred" $\overline{\delta c/c}$ to the non-zero exact sound-speed difference beneath the models' convection zones. Even when the reference and unknown models' convection zone depths are almost identical, $\delta c/c$ is non-zero beneath the convection zone because the physics in the non-convective interior is different, at least in the particular case under consideration here. Because of the smoothing, this affects $\overline{\delta c/c}$ in the region over which $\overline{\delta W}$ is calculated. If the smoothing parameter d is decreased, the errors in $\overline{\delta c/c}$ and its derivative in the region of interest are also decreased, so that the depth determined from the zero intercept of $\overline{\delta W}$ is more accurate. If d is reduced from $0.07R$ to $0.05R$, for example, the error in the inferred depth is reduced from $6 \times 10^{-3}R$ to $4 \times 10^{-3}R$. The results for this case are shown with stars in Figure 4. To summarize, this is an error which comes about from a sensitivity to the physics of the unknown model in the region beneath the convection zone and is directly related to the resolution scale of the method; if the physics in the unknown model were essentially the same as in the reference models up to depth of order d beneath the convection zone, this error would be greatly reduced.

However, in the case of no smoothing ($d \to 0$), the "inferred" depth of $0.2722R$ is still in error by $1.0 \times 10^{-3}R$ (cf. the crosses in Figure 4). The source of this error, which is closely analogous to

that discussed above, is the sensitivity of $\overline{\delta W}$ to W in the region of depth Δ beneath the convection zone. Because of the possibility of different physics there, this can also introduce some error into the depth determination. This error can be reduced somewhat by reducing the value of Δ: thus with $\Delta = 0.01R$, for example, the error in this case is reduced to $4 \times 10^{-4}R$. The value of Δ used in the definition of $\overline{\delta W}$ can of course be chosen at will, and so could be taken even smaller than this; but for actual inversions of data with realistic errors we have found that there is little to be gained from taking Δ to be less than $0.01R$.

We have performed differential inversions for Model X using all the reference models discussed in § V*a*, and using 20, 28 and 36 knots in the spline fit for $H_1(w)$. From the results of Christensen-Dalsgaard *et al.* (1990) we estimate the effective widths of the averaging kernels at a radius of $0.7R$ for the 20- and 28-knot cases to be between $0.05R$ and $0.1R$, while the effective width for 36 knots should be somewhat smaller. Thus 36 knots should provide the best resolution and the depth determination least liable to systematic error arising from uncertainties in the physics of the non-convective interior. However, as the resolution is improved, the sensitivity to errors in the data (loosely speaking, the error magnification) tends to increase (e.g. Craig and Brown 1986; Christensen-Dalsgaard *et al.* 1990). Thus it is not obvious that the 36-knot inversion will necessarily give the most reliable depth determination. In fact, it will be seen below from the results of tests with realistic data errors that it is indeed advantageous to use as many as 36 spline knots.

Figure 5 shows the inferred $\delta c/c$ and W using three reference models with convection zone depths spanning that of Model X. The cases of 28 and 36 knots are illustrated. It can be seen that the effects of smoothing for the 28-knot case are similar to those produced in Figure 3 with $d = 0.07R$. As expected, the resolution with 36 knots is rather better than with 28 knots. Of course, the true averaging kernels are more complicated than the averages described by equations (5.1) and (5.2); this accounts for the difference between the actual inversion results in Figure 5 and the results of artificial smoothing shown in Figure 3.

Figure 6 shows $\overline{\delta W}$ plotted against depth of convection zone for the X.1 data set (i.e., Model X with realistic errors) and all the reference models, using 36 knots and $\Delta = 0.01R$. A linear fit to these results implies a depth of $0.2725R$, which is in error by $1.3 \times 10^{-3}R$. (The linear behaviour of $\overline{\delta W}$ holds only for sufficiently small values of $\overline{\delta W}$; thus in all cases, only those points with $\overline{\delta W} < 0.02$ have been included in the linear interpolation. This means that approximately eight points have been used in each linear fit.) The results in Figure 6 are close to lying on a single curve, indicating that the determination is indeed largely insensitive to the detailed physics of the reference models. This has also been checked by using subsets of the reference models for the interpolation.

The results for all the other error realizations, and for inversions using 20 and 28 knots, are summarized in Table 5; the 20-knot inversions were carried out by author C in a blind test. Note that even with 36 knots, when one expects the error magnification to be greatest (cf. Christensen-Dalsgaard *et al.* 1990), the results are fairly insensitive to the errors in the data. The accuracy of the inferences is in good agreement with the predictions of the crude artificial smoothing model.

The exact and inferred sound-speed differences between Model X (with no errors) and a reference model with similar depth of convection zone (model 6 of Table 4) are shown in Figure 7a. It should be remarked that the accuracy of better than 0.2 per cent of the solar radius in the convection zone depth determination has been achieved in spite of the rather large differences in sound speed in the outer layers, which arise from the differences in composition between Model X and the reference models. It might also be noted from this figure that there is indeed a sudden increase in $\delta c/c$, reflecting the higher opacities in Model X, immediately beneath the convection zone. This is the principal source of the resolution-related error in the depth determination, as discussed above.

The results for Model Y are also summarized in Table 5. For this model the error in the inversion is less than $2 \times 10^{-3}R$ in all but one case. Once again the 20-knot inversions were performed in a blind test. The resolution-related error can most clearly be discerned in the results for the error-free data set Y.0; the error is small for this model, even with the poorest resolution, because the

increase in $\delta c/c$ beneath the convection zone is much more moderate in this case than in the case of Model X (cf. Figure 7b). It may also be noted that the difference between the results for error-free data and those for data with errors tends to increase with increasing number of spline knots, which is consistent with the expectation that the error magnification will increase as the resolution is improved.

Our inversions of artificial data also indicate that the sound speed at the base of the convection zone can be accurately inferred by the differential method. This enables one to estimate the temperature there (see § VII), which is of importance to the issue of lithium burning. For Model X, the depth of the convection zone is $0.2712R$ and the sound speed (c_b) at that depth is $2.144 \times 10^7 \mathrm{cm\,s^{-1}}$. The 36-knot inversion of data set X.0 gives a value of $2.145 \times 10^7 \mathrm{cm\,s^{-1}}$ at the exact location of the base of the convection zone; and this value does not change by more than $0.002 \times 10^7 \mathrm{cm\,s^{-1}}$ even using the data set with largest errors and the 20-knot inversion. The Model Y inversions give even more accurate results. Thus the accuracy of the determination of c_b is very high if d_b is known exactly. Of course for the Sun we do not know d_b exactly, and have to use the value inferred from inversion. Thus the uncertainty in the value of d_b introduces uncertainty in the determination of c_b. From equation (1.3) one can estimate that near $r = 0.7R$, $|Rd\ln c/dr| \simeq 2.4$; thus if the error in d_b is $\sigma(d_b)$, and the corresponding contribution to the error in the determination of c_b is $\sigma(c_b)$, we estimate that $\sigma(c_b)/c_b \simeq 2.4\sigma(d_b)/R$. This is in accordance with the results of the inversions. In all cases we have used the reference model with depth d_b most nearly matching the inferred value when inferring the sound speed. For data set X.0 and the inversion using 36 knot and $\Delta = 0.01R$, for which the inferred value of d_b is in error by $9 \times 10^{-4}R$, the inferred value of c_b is $2.150 \times 10^7 \mathrm{cm\,s^{-1}}$. For the corresponding inversion of the X.1 data, d_b is in error by $1.3 \times 10^{-3}R$ and the inferred c_b is $2.154 \times 10^7 \mathrm{cm\,s^{-1}}$. These results indicate that the dominant source of uncertainty in the determination of c_b is the uncertainty in the value of d_b.

c) Evaluation of errors in the differential depth determination

From the results of the numerical experiments described in the previous section, one can make estimates of the likely error in the determination of d_b from real solar data. We consider only the 36-knot, $\Delta = 0.01R$ determination, which provides our most accurate results. First there is an error which comes from errors in the data set. Assuming that these have been adequately represented in our experiments, this error can be estimated by comparing the results from data sets containing realistic errors, in particular sets X.1, X.2 and Y.1, with those from error-free data, X.0 and Y.0. In this way we estimate the error in d_b from data errors to be $\pm 0.002R$. This estimate includes the effect of a possible systematic scale-error in the high-degree data, as included in the X.1 data set.

The effect on the determination of d_b of random and systematic errors in the frequencies can also be estimated by noting that the inferred sound-speed difference can be expressed explicitly as a linear combination of the data (cf. Christensen-Dalsgaard *et al.* 1990):

$$\frac{\overline{\delta c}}{c}(r_0) = \sum_{n,l} d_{nl}(r_0) \left.\frac{\delta\omega}{\omega}\right|_{n,l} . \tag{5.5}$$

Thus the sensitivity of the sound-speed inversion at some radius to any particular mode is given by the coefficients d_{nl}. These are shown in Figure 8 for $r_0 = 0.65R$ and $r_0 = 0.75R$; the determination of the depth of the convection zone is only sensitive to the sound-speed inversion in this range (cf. equation (5.4)). The sound-speed inversion at these depths depends strongly on modes whose lower turning points lie in the vicinity; but modes of degree greater than 100, for which $\nu/L < 50\mu$Hz, make essentially no contribution at $r = 0.65R$, and only a modest contribution at $r = 0.75R$. Thus the depth determination should be insensitive to reasonable systematic errors in these modes. This is particularly important in the light of the suspected systematic errors in the observed frequencies at high degree (cf. § VI*b*). Furthermore the behaviour of the d_{nl} explains the insensitivity of the inversion to the inclusion of systematic errors in the frequencies of Model X (cf. Table 5).

A second source of error in the depth determination is that the physics in the reference models may not adequately represent the physics of the Sun. Thus it can be seen from Table 5 that even with error-free data the inferred depth of Model X is in error by nearly $0.001R$. Experiments with artificial smoothing (see § V*b*) support the conclusion that the principal source of this error is that Model X is hotter just below the convection zone than any of our reference models of comparable depth d_b. There is no evidence that the Sun is as extreme as Model X in this respect (cf. § VI*b*), so that in the Sun's case this particular contribution to the error is probably small, as it is for Model Y (cf. the determination for Y.0 in Table 5). Another way of seeking a possible model-dependent contribution to the error in d_b is to use different subsets of the reference models in the linear fit to $\overline{\delta W}$. We have compared the depths inferred using just the models 5 - 10 with CT opacities with those inferred using just the models 11 - 15 with LAOL opacities. For none of the 36-knot inversions do the two depths so inferred differ from one another by more than $5 \times 10^{-4}R$. (This is true also for the inversion of solar data discussed in § VI). Taking all this evidence together, we conclude that the error arising from the use of incorrect physics in the reference models is, in the case of the Sun, unlikely to exceed $0.001R$.

A particular problem concerns the description of the structure and oscillations in the outermost parts of the convection zone, and the solar atmosphere. Here the adiabatic approximation, which we have used in the calculation of oscillation frequencies for unknown and reference models, is certainly invalid, and there are likely dynamical effects, which we have also ignored, of convection. This could introduce errors, which are not reproduced in the tests reported here, in the inversions for solar sound speed. Indeed comparisons of observed and computed frequencies show evidence of a dominant contribution to the frequency errors from this region (e.g. Christensen-Dalsgaard, Däppen and Lebreton 1988). Since these effects are concentrated very near the solar surface, they are largely absorbed in the frequency-dependent part $\overline{H}_2(\omega)$ of the fit to equation (2.5). In fact, it is shown below (cf. Figure 9) that $\overline{H}_2(\omega)$ accounts for a substantial part of the frequency differences

between the observations and reference model 13. Estimates of the frequency changes caused by nonadiabaticity or by convective fluctuations (e.g. Balmforth and Gough 1990) indicate that they are of a similar magnitude, and have a roughly similar dependence on frequency and degree, as the effects of the opacity increase in the solar photosphere in the LAOL tables relative to the CT tables. In fact, the effect of the opacity change is concentrated in the same thin region near the surface where the structure, and the physics of the oscillations, are uncertain, and hence very likely affects the frequencies in a qualitatively similar way. We note that the use of reference models 11 - 15, which are based on the LAOL opacities, introduced no substantial error in the determination of d_b for the unknown Model Y, for which the CT opacities were used; hence it is likely that the neglected physical effects near the solar surface would make a similarly small contribution to the error in d_b.

To summarize, our estimate of the standard error in the differential determination of the depth of the Sun's convection zone is $\pm 0.003R$.

d) Other inferences from the data.

In addition to determining the convection zone depth, the observer using the differential method (author C) attempted to infer other properties of the artificial data and the underlying models. Estimates of the error properties of the data should in principle be taken into account in the inversion. Furthermore, from the inferred properties of the Sun it might be possible to select more appropriate sets of reference models. The present inversions did not incorporate such refinements; but it is of interest to see to what extent they would have been possible.

The results are discussed here solely on the basis of the notes that were communicated to Author A during the blind tests, and before a new data set had been transmitted. Although the results are somewhat incomplete, a comparison of the inferences with the actual properties of the data provides some insight into the diagnostic potential of solar oscillation data of this nature.

i) Systematic errors.

Author C found a sudden onset of systematic errors in mode set X.1 at $l = 110 - 120$; the relative magnitude of the error was estimated to be 1.5×10^{-3} in this region. This is in reasonable agreement with the actual systematic error, with a relative magnitude of 2.5×10^{-3}, starting from $l = 120$. Author C correctly inferred that there was no sudden onset of systematic errors in any of the other data sets.

ii) Random errors.

The properties of the random errors were described in terms of the variation with degree in the average standard deviation, between frequencies of 2.5 and 3.5 mHz, and the frequency dependence of the standard deviation at low degree. Author C gave no detailed description of the errors; however, the inferred general behaviour of the errors, particularly as a function of l, is in reasonable agreement with the actual values. As a fairly typical example we may consider mode set X.1. Here the relative standard deviation in frequency, scaled by $S(w)$ (cf. equation (2.4)) was estimated to be around 3×10^{-4} for $l = 0 - 100$, 6×10^{-4} at l around 300, 1.2×10^{-3} at l around 500, and even higher at higher l. The actual scaled relative standard deviations at a frequency of 3 mHz are $2.5 - 3.2 \times 10^{-4}$ for $l = 0 - 100$, 7×10^{-4} at $l = 300$, 1.0×10^{-3} at $l = 500$, and increasing to 1.7×10^{-3} at $l = 1000$. The variation with frequency at low degree was recovered somewhat less successfully, although author C correctly inferred that the standard deviation increases with frequency at high frequency.

A similar level of success was achieved for the other mode sets. In particular it might be noted that for $l > 100$ the errors in mode set Y.2 were correctly found to be about 1/3 of the errors in mode set Y.1 (as a result of the smaller value of w^* in the latter set; cf. Table 2).

iii) Other properties of the models.

Author C attempted a fairly careful analysis of the properties of Model Y. From the behaviour of $\overline{H}_2$ resulting from the comparison with reference model 1, as well as the behaviour of the sound-speed

difference resulting from the inversion in the outermost layers of the model, he correctly inferred that physics of the outer layers of Model Y was similar to reference model 1, and that in particular the equation of state was very similar to EFF. He also estimated that the envelope helium abundance in Model Y was 0.256 ± 0.01, on the basis of a comparison with reference models 1 and 3; this is consistent with the correct value of 0.249.

The frequency separations $\nu_{n,0} - \nu_{n-1,2}$ and $\nu_{n,1} - \nu_{n-1,3}$, where $\nu_{n,l}$ is the frequency of a mode of order n and degree l, are sensitive to the variation of the hydrogen abundance in the solar core (e.g. Provost 1984; Faulkner, Gough and Vahia 1986; Christensen-Dalsgaard 1986). By considering these separations, author C concluded that there had been some mixing of the core of the model, to an extent roughly intermediate between a standard model and the Schatzman *et al.* (1981) partially mixed model with $Re^* = 100$. A similar conclusion was reached on the basis of the behaviour of the sound-speed difference in the core of the model (cf. Figure 7b). As described in § III the core hydrogen abundance is in fact precisely halfway between the standard and the $Re^* = 100$ model. From the corresponding sound-speed difference for Model X (Figure 7a) author C correctly found no evidence for mixing in that model.

VI. ANALYSIS OF OBSERVED FREQUENCIES

a) Results of absolute inversion

The solar data of Duvall *et al.* (1988) and Libbrecht and Kaufman (1988) (see § III) were inverted in the manner described in § IV. The depth d_b inferred by this method is $0.279R$. In the light of our experiments with artificial data, we therefore infer from the absolute inversion that the depth d_b of the solar convection zone is $0.279(\pm 0.010)R$.

b) Results of differential inversion

The inversion of the solar data was performed in the same way as in the tests described in § V. Figure 9a shows scaled differences between observed frequencies and those of the reference model (model 13) which appears to match the Sun most closely in terms of the depth of its convection zone. The residuals after the spline fit for $H_2(\omega)$ has been removed are shown in Figure 9b. The range of variation of the residuals is considerably smaller than that of the original scaled differences, indicating that much of the difference in frequencies between the model and the Sun comes from the surface layers. There is some spread in the residuals about the spline fit for $H_1(w)$ (Figure 9b). Experiments with artificial data suggest that departures from the asymptotic expression (2.5) account for only a small part of this; thus the main contribution to the residual spread is probably errors in the reported frequencies. There appears to be a slight mismatch between the two data sets in the vicinity of $\nu/L = 25\mu$Hz, as remarked by Christensen-Dalsgaard, Gough and Thompson (1988) using a similar analysis. They suggested that the high-degree data, which are obtained from fitting to ridges in the power spectra, might contain some systematic scaling error. The low-degree frequencies, which are found by identifying individual modes, are probably less susceptible to such errors. That the high-degree data contained errors has been confirmed independently by Libbrecht (private communication). However, as discussed in § V*c*, modes with $l \geq 100$ carry relatively little weight in the differential sound-speed inversion for $r \leq 0.75R$, and hence have little effect on the determination of the depth of the convection zone.

The differential inversion was carried out using 20, 28 and 36 knots in the spline fit for H_1. Figure 10 shows the resulting inferred sound-speed difference relative to reference model 13. Near the base of the convection zone the results are fairly insensitive to the number of knots. The features in $\delta c/c$ in the outer convection zone might reflect some error in the equation of state, but they could also arise from systematic errors in the high-degree data, to which the inversion in this region is very sensitive.

The depth of the convection zone inferred from each of these inversions is given in Table 6. There is little variation from one inversion to another, in contrast with Model X but like Model Y. Moreover, there is no evidence in the sound-speed inversion for any steep change in $\delta c/c$ beneath the convection zone, as exhibited in the inversions for Model X. Thus we would expect the test inversions for Model Y in particular to be a good guide to the likely error in our determination. We therefore infer from the differential inversion that the depth of the solar convection zone is $0.287(\pm 0.003)R$.

We note that the depth inferences from the two methods we have employed are consistent, in that the more precise (and, we hope, more accurate) differential inference is within the error bars of the absolute determination.

As discussed at the end of § V*b*, the differential inversion also enables us to obtain the sound speed c_b at the base of the convection zone, with an uncertainty that comes principally from the uncertainty in d_b. The values we infer for c_b from the various inversions are listed in Table 6. We estimate that $c_b = 2.233(\pm 0.020) \times 10^7 \mathrm{cm\,s^{-1}}$.

VII. OTHER PROPERTIES AT THE BASE OF THE CONVECTION ZONE

Having determined c_b directly from the inversions, the temperature T_b at the base of the convection zone can also be estimated, using the perfect gas law (4.4), as

$$T_b = \frac{\mu}{\gamma \mathcal{R}} c_b^2. \tag{7.1}$$

The mean molecular weight depends principally on the helium abundance Y: indeed, for a fully ionized gas

$$\mu \simeq \frac{1.008}{2 - 1.245Y - 1.5Z}, \tag{7.2}$$

where Z is the abundance of elements heavier than helium, and we have assumed a value of 0.5 for the ratio between the total number of particles (nucleus plus unbound electrons) and atomic mass for the heavy elements. In this case, furthermore, $\gamma = 5/3$.

These expressions evidently depend on the assumption that the equation of state of the gas can be adequately represented by a fully ionized ideal gas. Indeed, solar models indicate that only about 1 per cent of the electrons are bound at the conditions corresponding to the base of the convection zone. This effect, and non-ideal effects in the gas, give rise to errors in T_b of less than 1 per cent. Furthermore, for all reference models in Table 4 $\gamma = 1.664$ at the base of the convection zone. Thus the principal uncertainties in the determination of T_b come from the uncertain chemical composition, in particular the helium abundance Y, and the uncertainty in the value of c_b. It follows from linearizing equation (7.2) about $Y = 0.26$, and taking $Z = 0.02$ and $\gamma = 1.664$, that

$$T_b = 2.21(\pm 0.04) \times 10^6 [1 + 0.76(Y - 0.26)]\mathrm{K}. \tag{7.3}$$

The uncertainty of $\pm 0.04 \times 10^6$K comes from the uncertainty in c_b.

To date a reliable direct determination of the solar helium abundance has not been possible. Therefore one must resort to obtaining Y from calibration of solar models. As remarked in Table 4, the outcome depends in particular on the opacities used, since the constraint on the luminosity provides a relationship between composition and opacity in the deep interior; for a given opacity table, this fixes μ in the convection zone. Interpolating in the table to models with the inferred d_b, we find that $Y = 0.237$ and 0.285 for the CT and the LAOL opacities, respectively. Based on measurements of the helium abundance in other astrophysical systems as well as on evidence from cosmology it appears unlikely that Y deviates substantially from the range 0.23 to 0.30 (e.g. Boesgaard and Steigman 1985; Pagel 1989). According to equation (7.3) this corresponds to T_b being in the range $2.12 - 2.32 \times 10^6$ K; the uncertainty in c_b and the assumed range in Y contribute roughly equally to the uncertainty in T_b. We emphasize that given an improved determination of Y a more accurate estimate of T_b can be obtained from equation (7.3).

Alternatively, given d_b one can estimate the temperature at the base of the solar convection zone from solar models. Figure 11 illustrates the dependence of T_b on d_b, and on the physics of the

models, in the reference models in Table 4. These dependencies may be understood by noting that from the approximate expression (1.3) for c^2 and equation (7.1) we obtain

$$T_b \simeq (1 - \gamma^{-1}) \frac{\mu G M}{\mathcal{R} R} \left(\frac{R}{r_b} - 1 \right). \tag{7.4}$$

One can estimate the solar value of T_b by determining what the values would be for models constructed with the same physical assumptions as the reference models and with d_b as determined for the Sun. In Figure 11 the shaded region indicates the inferred range of the solar value of d_b; from this one would estimate that T_b is in the range $2.15 - 2.30 \times 10^7 \mathrm{cm\,s^{-1}}$. Given that the temperature at the base of the convection zone is essentially determined by Y and d_b, and that the range of Y found in our reference models is contained in, but somewhat smaller than, the range assumed for our previous estimate of T_b, it is not surprising that the estimate based on Figure 11 results in a smaller range in T_b.

It is also of some interest to estimate the mass Δm_b contained within the convection zone. The relation between Δm_b and the depth of the convection zone depends on the physics of the model, in particular the opacity. From a graph similar to Figure 11 we estimate that Δm_b is 2.2 ± 0.2 per cent of the solar mass.

VIII. DISCUSSION

In traditional solar models there is an essentially discontinuous transition at the base of the convection zone between very nearly adiabatic and purely radiative stratification. To within the spatial resolution of our inversions, the Sun is no different. This is illustrated by the scaled sound-speed gradient W defined in equation (1.4); as shown in Figure 10b the behaviour of $W(r)$ inferred from the Sun's oscillation frequencies is very similar to that in a theoretical model for which the convection zone has approximately the same depth. The location of the transition from adiabatic

to subadiabatic stratification marks what we define as the bottom of the convection zone, for which we infer a depth d_b of $0.287(\pm 0.003)R$.

Our estimate of the uncertainty in the determination of d_b is based on tests of the analysis methods, carried out partly in a blind fashion. These used artificial data from two equilibrium models, the structures of which were not known to those authors carrying out the analysis, with rather different physics. The data were obtained by adding to the computed adiabatic frequencies for these models various realizations of simulated errors, including some with standard deviations based on those estimated for the observed data. In addition to errors in the data, the differential inversion method could in principle be sensitive to errors in the equilibrium structure of the reference models employed. However, despite considerable differences in physics or chemical composition between the reference and the unknown models, the analysis recovered the convection zone depths of the latter with considerable accuracy; furthermore there was little difference in the inferred values of d_b based on subsets of reference models with different physics, both in the case of the unknown models and for the observed frequencies. It might be noted that although the frequency computations neglected uncertain aspects of the physics of the oscillations concentrated near the solar surface, such as nonadiabaticity and effects of convection, the range of differences between unknown and reference models was probably sufficiently large to simulate the likely effects of these uncertainties.

One possible source of error in our determination of r_b could be the presence of a layer of magnetic field immediately beneath the convection zone. The effect can be crudely estimated as follows. If a field were present, the modification to the wave equation would be roughly to replace c^2 by $c^2+{v_A}^2$, where v_A is the Alfvén speed averaged over horizontal surfaces. Immediately beneath the convection zone, where $d{v_A}^2/dr$ would be negative, the apparent value of W would be diminished; thus it could remain at approximately $-2/3$ for a distance d, which would be the amount by which we would have overestimated the depth of the convection zone. At greater depths, $d{v_A}^2/dr$ would be

positive, and the field would cause W to rise more rapidly with depth until it reaches the field-free value as ${v_A}^2$ diminishes to a negligible value. For the field to cause this error would require

$$\frac{r^2}{GM}\frac{d}{dr}\left(c^2+{v_A}^2\right) = W + \frac{r^2}{GM}\frac{d{v_A}^2}{dr} \simeq -2/3 \tag{8.1}$$

in the region of the radiative interior that we would falsely infer to be convective. In that region, W is given by equation (4.12). Assuming $v_A = 0$ at $r = r_b$ equation (8.1) then implies that

$${v_A}^2 \simeq \frac{GM}{R}\left\{\left[\frac{2}{3}-\gamma(1-\Gamma^{-1})\right](\xi-\xi_b) - \gamma(1-\Gamma^{-1})\int_{\xi_b}^{\xi}\xi'\frac{df}{d\xi'}d\xi'\right\}, \tag{8.2}$$

where $\xi_b = \xi(r_b)$. This yields, at the base $r = r_b - d$ of that region, a magnetic field B given (in Gauss) by

$$B \simeq 0.4\left(\frac{4\pi a G M\rho}{R}\right)^{1/2}\frac{d}{R} \simeq 8\times 10^7\frac{d}{R}, \tag{8.3}$$

in which we have used the Kramers value of 8.5 for the constant a and we have assumed $\rho \simeq 0.2\mathrm{g\,cm^{-3}}$. Thus, for example, an appropriately confined magnetic field of 1 MG would have caused us to overestimate d_b by 1 per cent of the solar radius. It would not be necessary for the field to be distributed precisely as required by equation (8.2), because the resolution of our inversions does not permit us to measure details on a scale less than about $0.02R$.

Notice that the presence of a field would not cause us to underestimate the depth: for the derivative of the inferred W to be negative within the lower layers of the convection zone it would be necessary that $d{v_A}^2/dr < 0$, which would require a substantial slowly varying field throughout the remainder of the convection zone in order to keep the deviation from $-2/3$ of our inferred W below a perceptible level.

At present there is no compelling evidence for the existence of a magnetic field at the base of the solar convection zone. However we note that a field of a few megagauss localized to this region has been proposed to explain certain features of the observed spectrum of p-mode frequencies (Thompson 1988; Dziembowski and Goode 1989).

Both our methods are derived from the same asymptotic formula (2.1) for the oscillation frequencies, but the other assumptions on which they are based are quite different. The absolute method uses only on the formula itself, and does not rely directly on a theoretical model of the Sun. Although the differential sound-speed inversion method depends on a reference model, we have previously shown (Christensen-Dalsgaard, Gough and Thompson 1989) that the sound speed can be determined quite accurately even when the unknown model and reference model differ considerably. However, the inferred sound-speed difference $\overline{\delta c/c}$ is perforce a smooth function of radius; any sharp features in the sound speed $c(r)$ of the reference model therefore tend to persist in the inferred sound speed $(1+\overline{\delta c/c})c(r)$. This is a hindrance for our present purpose, where we seek to identify the base of the convection zone by locating a near-discontinuity in the sound-speed gradient. For this reason we have performed what amounts to a calibration of the Sun against a collection of theoretical models, utilizing the results of differential sound-speed inversions. Of course the method calibrates only a very limited aspect of the models, essentially only the sound speed in the vicinity of the base of the convection zone. Therefore, even though the method as implemented uses complete solar models, our determination of d_b is hardly influenced, for example, by errors in our modelling of the uncertain structure of the radiative interior or of the surface layers.

Such insensitivity to the reference models is not necessarily a property of estimates of a quantity such as temperature, which cannot be determined directly by seismology. The relationship between sound speed and temperature depends on the composition and the thermodynamic state of the gas, which must be inferred by other means. At the base of the convection zone the perfect gas law (4.4) is satisfied quite well, and the most abundant elements are almost fully ionized; therefore $\gamma \simeq 5/3$ and the mean molecular weight is quite simply represented in terms of the helium abundance Y. Given that the sound speed at the base of the convection zone has now been determined, a knowledge of Y would enable one to determine the temperature T_b there. One may hope that in future the value of Y will be determined seismologically in the HeII ionization zone (Däppen and Gough 1984).

Indeed, Y has been inferred to within 0.01 from the frequencies of unknown theoretical models (Däppen, Gough and Thompson 1988; see also § V*d*). Since at least the adiabatically stratified part of the convection zone is indisputably chemically mixed, this will provide the most important missing information for determining T_b. Until then we are forced to depend on solar models and on evidence from other areas of astrophysics and cosmology to restrict the range of possibilities.

Typical values of d_b for evolution models computed with the "standard" assumptions of stellar structure are given in Table 4, for reference models 1 – 4. When the Cox and Tabor opacities are used, the results are quite close to those obtained from helioseismology (models 1 and 2). On the other hand, use of the more modern Los Alamos Opacity Library (LAOL) yields models with substantially too shallow a convection zone, and a temperature T_b of only 2.0×10^6 K at its base (models 3 and 4). The recent "standard" solar models of Bahcall and Ulrich (1988) and Turck-Chièze *et al.* (1988) share this deficiency. It is only after artificially modifying the opacities derived from LAOL that the correct value of d_b is achieved. For the parameters we have chosen this requires the maximum fractional increase in opacity (which occurs for $T \leq T_2 \simeq 4 \times 10^6$ K) to be 28 per cent, which is roughly consistent with the findings of Cox, Guzik and Kidman (1989) and Korzennik and Ulrich (1989). To maintain that the LAOL opacities are nonetheless close to the truth requires modification of other aspects of the model to reconcile the depth of the convection zone with what is now measured. Indeed, it follows from equation (8.3) that a large-scale megagauss magnetic field just beneath the base of the convection zone might account for the difference between the seismically inferred value of d_b and the value obtained in the LAOL models. In any case, when comparing the inferred solar value of d_b with that resulting from "standard" solar models it must be kept in mind that in the latter the adiabatic stratification only extends over the region that is unstable to convection. The increase in the depth of the adiabatically stratified region required for the LAOL models is approximately one quarter of the pressure scale height at the base of the convection zone; we note that this is not inconsistent with estimates of the extent of the overshoot region (van Ballegooijen 1982; Schmitt,

Rosner and Bohn 1984; Roxburgh 1985; Pidatella and Stix 1986), although it should be emphasized that such estimates are currently uncertain. If overshoot does not cause a significant adjustment to Y, one would then infer from Figure 11 that the temperature at the base of the convection zone is actually in the range $2.23 - 2.29 \times 10^6$K.

From our estimates of T_b, and using the cross section measured by Rolfs and Kavanagh (1986), we deduce that the e-folding time for depletion of ^{7}Li at the base of the convection zone currently exceeds 4×10^{10} years. According to the computed evolution sequences the temperature at the base of the convection zone has decreased by about 10 per cent since the Sun arrived on the Zero-Age Main Sequence. Even so, the reduction by about a factor of 100 of the observed solar surface lithium abundance relative to the normally assumed cosmological value, or to the abundance in meteorites, can only be achieved either through substantial lithium burning in the pre-main-sequence phase or through additional mixing of the radiative interior (e.g. Baglin, Morel and Schatzman 1985; Lebreton and Maeder 1987).

IX. CONCLUSION

The base of the adiabatically stratified region of the solar convection zone is at a radius $r_b = 0.713 \pm 0.003R$, where R is the radius of the Sun; thus the depth of the convection zone is $d_b = 200 \pm 2$ Mm. The sound speed at $r = r_b$ is 0.223 ± 0.002Mms^{-1}. The corresponding value of the temperature T_b at the base of the convection zone depends on the chemical composition of the convection zone. If the helium abundance Y is in the range 0.23 - 0.30, we conclude that T_b lies in the range $2.12 - 2.32 \times 10^6$ K. For other values of Y, T_b would be given by formula (7.3). We also deduce by comparison with solar models that the Sun's convection zone contains 2.2 ± 0.2 per cent of the solar mass.

ACKNOWLEDGEMENTS

We are grateful to Y. Lebreton for helping to install new physics in the program utilized in computing the models used in this paper. We thank P. A. Gilman, J. Madsen, P. E. Nissen and D. Schmitt for helpful discussions, and T. M. Brown for commenting on an earlier version of the paper. We are grateful to the Institute for Theoretical Physics, Santa Barbara, for hospitality during the later phases of the preparation of the paper. ITP is supported by the National Science Foundation under Grant No. PHY82-17853, supplemented by funds from the National Aeronautics and Space Administration.

APPENDIX A: SOUND SPEED NEAR THE BASE OF THE CONVECTION ZONE

(i) Stratification of the lower regions of the convection zone

We presume that the matter is fully ionized, so that γ is constant and thus

$$p = K\rho^{\gamma}, \tag{A1}$$

where K is a constant. Let

$$m(r) = M[1 - \epsilon(r)]; \tag{A2}$$

$\epsilon(r)$ is small ($\lesssim 0.02$) throughout the convection zone. Then the equation of hydrostatic support

$$\frac{dp}{dr} = -\frac{Gm\rho}{r^2} \tag{A3}$$

can be integrated to give

$$c^2 \equiv \frac{\gamma p}{\rho} = (\gamma - 1)\frac{GM}{R}\left(\tilde{\xi} + R\int_R^r \frac{\epsilon(r')}{r'^2}dr'\right), \tag{A4}$$

where

$$\tilde{\xi} = \frac{R}{r} - \frac{R}{r_c},$$

and r_c is a constant radius which for the Sun is very close to R.

To a first approximation, $\tilde{\xi}$ is the fractional depth, so ignoring the term in ϵ equations (A1) and (A4) give

$$\rho \simeq \rho_0\tilde{\xi}^n, \tag{A5}$$

where $n \equiv 1/(\gamma - 1) = 1.5$ in the lower convection zone. This approximation can then be used to evaluate ϵ:

$$-M\,d\epsilon = dm = 4\pi r^2\rho dr \simeq -\frac{4\pi}{R}r^4\rho d\tilde{\xi},$$

so

$$d\epsilon \simeq \frac{4\pi R^3}{M}\rho_0\tilde{\xi}^n(1-\tilde{\xi})^4 d\tilde{\xi}. \tag{A6}$$

Equation (A4) can be rewritten as

$$c^2 \simeq (\gamma - 1)\frac{GM}{R}(1 - e\epsilon)\tilde{\xi} \tag{A7}$$

where

$$e \equiv (\epsilon\tilde{\xi})^{-1}\int_0^{\tilde{\xi}} \epsilon(\xi')d\xi', \tag{A8}$$

which can be computed by integrating equation (A6). Evaluated near the base of the convection zone (where $\tilde{\xi} \simeq 0.4$), $e \simeq 0.25 + 0.38\tilde{\xi} \simeq 0.4$; moreover, ϵ is small, so equation (A7) yields

$$c^2 \simeq (\gamma - 1)\frac{GM}{R}\left(\frac{R}{r} - \frac{R}{r_c}\right)\left(\frac{m}{M}\right)^e. \tag{A9}$$

(ii) Stratification of the outer layers of the radiative interior

We assume that γ and μ are constant, and that

$$\frac{dT}{dr} = -\Lambda\frac{\rho^{1+\lambda}T^{-(3+\nu)}}{r^2} \tag{A10}$$

where Λ, λ and ν can also be treated as constants. Suppose further that variations in m with radius can be neglected, and that the equation of state can be represented by the perfect gas law (equation 4.4). Then equation (A10) and the equation (A3) of hydrostatic support yield an equation for dp/dT which can be integrated to give

$$p^{1+\lambda} \simeq \frac{1+\lambda}{a}\frac{Gm}{\Lambda}\left(\frac{\mathcal{R}}{\mu}\right)^{\lambda} T^a\left[1 + \left(\frac{T_0}{T}\right)^a\right] \tag{A11}$$

where T_0 is a constant and

$$a = 4 + \lambda + \nu. \tag{A12}$$

It is presumed (and can be verified *a posteriori*) that T_0/T is small in the region of interest. Equation (A11) can be solved for T/T_0 in terms of ρ/ρ_0, where ρ_0 is another undetermined constant:

$$\frac{T}{T_0} \simeq \left(\frac{\rho}{\rho_0}\right)^{(1+\lambda)\eta}\left[1 - \eta\left(\frac{\rho}{\rho_0}\right)^{-(1+\lambda)\Gamma}\right]. \tag{A13}$$

Here

$$\eta = 1/(3+\nu); \qquad \Gamma = \frac{4+\nu+\lambda}{3+\nu}. \tag{A14}$$

Equations (A11) and (A13) can be rearranged to give p in terms of ρ (and constants p_b, ρ_b):

$$\frac{p}{p_b} \simeq \left(\frac{\rho}{\rho_b}\right)^{\Gamma} \left[1 - \eta\left(\frac{\rho}{\rho_0}\right)^{-(1+\lambda)\Gamma} - \frac{\nu+2\lambda+4}{2}\eta^2\left(\frac{\rho}{\rho_0}\right)^{-2(1+\lambda)\Gamma}\right]. \tag{A15}$$

Substituting this expression into equation (A3) and integrating then yields

$$\frac{Gm}{R}\xi = \tag{A16}$$
$$\frac{\Gamma}{\Gamma-1}\left(\frac{\rho}{\rho_b}\right)^{\Gamma}\frac{p_b}{\rho}\left[1 - \frac{\lambda\eta(\Gamma-1)}{1+\lambda\Gamma}\left(\frac{\rho}{\rho_0}\right)^{-(1+\lambda)\Gamma} - \frac{(1+2\lambda)(\nu+2\lambda+4)(\Gamma-1)}{2(2\lambda\Gamma+\Gamma+1)}\eta^2\left(\frac{\rho}{\rho_0}\right)^{-2(1+\lambda)\Gamma}\right].$$

Here

$$\xi = \frac{R}{r} - \frac{R}{r_0} \tag{A17}$$

and r_0 is a constant of integration. Eliminating (ρ/ρ_b) between (A15) and (A16) gives

$$c^2 = \frac{\gamma}{\Gamma}(\Gamma-1)\frac{Gm}{R}\xi\left(1 - \Xi + C\Xi^2\right) \tag{A18}$$

where

$$\Xi = \frac{(1+\lambda)\eta}{1+\lambda\Gamma}\left(\frac{\rho}{\rho_0}\right)^{-(1+\lambda)\Gamma} \tag{A19}$$

and C is a (known) constant depending on λ, Γ and η. Equation (A16) permits Ξ to be expressed in terms of ξ; so equation (A18) can be rewritten as

$$c^2 = \frac{\gamma}{\Gamma}(\Gamma-1)\frac{Gm}{R}\xi f(\xi) \tag{A20}$$

where

$$f(\xi) = 1 - \delta\xi^{-a} - A\delta^2\xi^{-2a}, \tag{A21}$$

$$A = \left(\frac{\lambda\Gamma+1}{\lambda+1}\right)^2\left[\frac{\nu-\lambda^2+1}{\lambda\Gamma+1} - \frac{(2\lambda+1)(2\lambda+\nu+4)(\Gamma-1)}{2(2\lambda\Gamma+\Gamma+1)}\right] \tag{A22}$$

and δ is a constant. When $\lambda = 1$, $\nu = 3.5$, appropriate to Kramers' opacity law, A takes the value 1.33.

(iii) Fitting at the base of the convection zone

Taking γ and m to be known adequately from models, equation (A20) expresses the sound speed as a function of radius in terms of four unknown constants, which may be taken to be λ, ν, δ and r_0. A fifth unknown, which does not enter equation (A20) but which is of primary significance for the present discussion, is the location r_b of the base of the convection zone. More conveniently, the five unknowns may be regarded as λ, ν, r_b, $\xi_b \equiv \xi(r_b)$ and $\hat{\delta} \equiv \delta\xi_b^{-a}$. Continuity of c^2, given by equations (A9) and (A20), and its derivative at the base of the convection zone gives two equations

$$(1 - \hat{\delta} - A\hat{\delta}^2)\xi_b = \left(\frac{R}{r_b} - 1\right)\frac{1-\gamma^{-1}}{1-\Gamma^{-1}} \equiv \left(\frac{R}{r_b} - 1\right)B, \tag{A23}$$

$$1 + (a-1)\hat{\delta} + (2a-1)A\hat{\delta}^2 = \frac{1-\gamma^{-1}}{1-\Gamma^{-1}} = B. \tag{A24}$$

(Here equation (A9) has been simplified by neglecting the deviation of $(m/M)^\epsilon$ from unity and by setting $r_c = R$, and we have approximated m by M in equation (A20)). Equation (A24) immediately gives $\hat{\delta}$ in terms of λ and ν:

$$\hat{\delta} = \frac{1 - a + \left[(a-1)^2 + 4(2a-1)(B-1)A\right]^{1/2}}{2(2a-1)A}; \tag{A25}$$

whence equation (A23) gives ξ_b in terms of λ, ν and r_b. The integration constant r_0 is then given by

$$r_0 = \left(\frac{R}{r_b} - \xi_b\right)^{-1} R. \tag{A26}$$

It approximates the radius the Sun would have had were it not for the convective envelope (it ignores ionization and deviations from the simple power-law approximation to the opacity).

The remaining unknowns, λ, ν and r_b, are estimated from the sound-speed inversion in the radiative interior. This procedure is discussed in § IV.

APPENDIX B: PROCEDURES FOR THE ABSOLUTE INVERSION.

The function $F(w)$ (cf. equation (2.1)) was estimated from the data by the procedure outlined by Gough (1986). First the I modes in the data set were placed in a linear sequence in order of

increasing w, and labelled with their position i in that sequence. Then $\alpha(\omega)$ was determined by iteration, by setting

$$\alpha(\omega) = \alpha_0 + \pi^{-1}\omega\phi(\omega;\alpha_0); \tag{B1}$$

here α_0 is a constant, and ϕ was initially set to zero, and was subsequently obtained from the preceding iteration. Introducing

$$F_i = \frac{\pi(n+\alpha_0)}{\omega_i} + \phi(\omega_i), \tag{B2}$$

α_0 was determined by minimizing

$$\sum_{i=2}^{I-1}(F_{i-1} - 2F_i + F_{i+1})^2, \tag{B3}$$

to make F as near as possible to a single-valued function of w. The resulting function was smoothed: $F \rightarrow \mathcal{S}F$, and then ϕ was redetermined by introducing a discrete mesh ω_j of ω and averaging equation (B2):

$$\phi(\overline{\omega}_j) = \frac{\sum[1 - \pi(n+\alpha_0)/\omega_i F_i]}{\sum F_i^{-1}}, \tag{B4}$$

$$\overline{\omega}_j = J^{-1}\sum \omega_i, \tag{B5}$$

the sums being over all J modes with frequencies within half a mesh interval of ω_j. Finally, F was recomputed from equation (B2) and transferred to a computational grid for inverting equation (2.2). In practice twenty equal mesh intervals in ω over the range $[\omega_{min},\ \omega_{max}]$ spanned by the data were used.

The smoothing of the function F was carried out using two passes of a cosine-weighted running mean over five modes: $\mathcal{S}F = \mathcal{M}^2F$, where

$$\mathcal{M}F_i = \sum_{i-2}^{i+2} v_{ij}F_j \Big/ \sum_{i-2}^{i+2} v_{ij}, \tag{B6}$$

with $v_{ij} = \cos[(i-j)\pi/6]$ if $1 \le j \le I$ and $v_{ij} = 0$ otherwise. Subsequently F was transferred to a new mesh, used for inverting the Abel equation, by means of uniformly weighted linear regression on all modes having w within half a mesh interval of the appropriate mesh point. The computational

mesh comprised 201 points, uniformly divided in $\log w$ between $c(R)/R$ and the greatest value for which there was an observation.

TABLE 1.

PROPERTIES OF THE UNKNOWN MODELS

Property	Model X	Model Y
Opacity table	LAOL	Cox and Tabor (1976)
Opacity modification:		
$\log T_1$	6.5	6.0
$\log T_2$	6.8	6.4
A	0.2	0.025
Hydrogen profile	Standard	Partially diffusively mixed
Surface luminosity	3.8×10^{33}ergs^{-1}	3.846×10^{33}ergs^{-1}
Envelope helium abundance	0.3390	0.2486
Depth of convection zone	$0.2712R$	$0.2793R$

NOTES.—LAOL refers to the Los Alamos Opacity Library (Huebner *et al.* 1977) supplemented by additional opacity sources near the surface. The opacity was modified according to equations (3.1) and (3.2), with the parameters $\log T_1$, $\log T_2$ and A specified in the table; in both cases $\Delta \log T$ was 0.2. Both models were constructed using the equation of state of Eggleton *et al.* (1973). The hydrogen profile in Model Y is intermediate between that of a normal model of the present Sun and the profile in the diffusively mixed model with $Re^* = 100$ of Schatzman *et al.* (1981).

TABLE 2

PROPERTIES OF THE ARTIFICIAL DATA

Frequency set	A_w μHz	w μHz	A_ν μHz
X.1	0.200	120.00	3.000
X.2	0.200	120.00	3.000
X.3	0.200	50.00	3.000
X.4	0.100	50.00	1.500
X.0	0.	...	0.
Y.1	0.200	120.00	3.000
Y.2	0.200	50.00	3.000
Y.3	0.100	50.00	1.500
Y.0	0.	...	0.

NOTES.—The sets labelled X.n and Y.n refer to unknown Models X and Y (cf. Table 1). For each model the frequency sets are distinguished by their error properties, as described by the parameters A_w, w^* and A_ν (cf. equations (3.3) and (3.4)); in all cases $\nu_{max} = 5000$ μHz was used. Note also that, as described in the text, set X.1 included systematic errors for modes of degrees exceeding 120. No errors were added to the sets X.0 and Y.0.

TABLE 3

RESULTS OBTAINED WITH THE ABSOLUTE METHOD

FOR ARTIFICIAL DATA

Frequency set	d_b/R	ν
X.1	0.2626	5.66
X.2	0.2680	5.66
X.3	0.2720	5.45
X.4	0.2710	5.45
X.0	0.2705	5.45
Y.1	0.2864	5.45
Y.2	0.2828	5.45
Y.3	0.2740	5.45
Y.0	0.2688	5.25

NOTES.—Frequency sets labelled X.n and Y.n refer to different error realizations for the unknown Models X and Y (cf. Table 2). The second and third columns give the fractional depth d_b/R of the convection zone and the temperature exponent ν of the opacity as inferred using the absolute method described in § IV. The exact values of d_b for Models X and Y are $0.2712R$ and $0.2793R$ respectively.

TABLE 4.

REFERENCE MODELS

Model no.	Equation of state	Opacity Table	Opacity A	Energy generation	Evolution or static	Y_0	d_b/R	T_b (10^6 K)
1	EFF	CT	0.	FCZ	E	0.2473	0.2825	2.140
2	MHD	CT	0.	FCZ	E	0.2371	0.2851	2.165
3	EFF	LAOL	0.	P	E	0.2821	0.2638	1.997
4	MHD	LAOL	0.	P	E	0.2724	0.2668	2.028
5	MHD	CT	-0.07	P	S	0.2260	0.2674	1.968
6	MHD	CT	-0.05	P	S	0.2284	0.2719	2.016
7	MHD	CT	-0.02	P	S	0.2320	0.2786	2.090
8	MHD	CT	0.	P	S	0.2343	0.2827	2.136
9	MHD	CT	0.04	P	S	0.2387	0.2905	2.225
10	MHD	CT	0.1	P	S	0.2452	0.3013	2.352
11	MHD	LAOL	0.05	P	S	0.2801	0.2751	2.126
12	MHD	LAOL	0.07	P	S	0.2821	0.2794	2.175
13	MHD	LAOL	0.1	P	S	0.2850	0.2857	2.247
14	MHD	LAOL	0.15	P	S	0.2895	0.2958	2.366
15	MHD	LAOL	0.2	P	S	0.2939	0.3055	2.483

NOTES.—EFF and MHD refer to the equations of state of Eggleton *et al.* (1973) and Mihalas *et al.* (1988) respectively. CT denotes the Cox and Tabor (1976) opacity tables, whereas LAOL refers to the Los Alamos Opacity Library (Huebner *et al.* 1977) supplemented by additional opacity

sources near the surface. Modifications to the opacity immediately beneath the convection zone were carried out according to equation (3.1), with $\log T_1 = 6$, $\log T_2 = 6.6$, and $\Delta \log T = 0.15$; the lower temperature T_1 was chosen to be well inside the convection zone, where the value of the opacity is irrelevant. The parameter A determines the amplitude of the opacity modification. The energy generation parameters were obtained from Fowler, Caughlan and Zimmerman (1975; FCZ), or Parker (1986) and Bahcall and Ulrich (1988) (P). In the column headed "evolution or static" E indicates that the model is the result of a full evolution calculation, whereas S indicates that the model was obtained by scaling a previously computed hydrogen abundance profile in the manner described in the text. The remaining columns give the computed properties of the models: Y_0 is the envelope helium abundance (which is equal to the presumed uniform zero-age helium abundance) obtained from the requirement that the model have the correct luminosity, d_b/R is the depth of the convection zone, in units of the solar radius, and T_b is the temperature at the base of the convection zone.

TABLE 5

RESULTS OBTAINED WITH THE DIFFERENTIAL METHOD

FOR ARTIFICIAL DATA

Frequency set	$\Delta = 0.01R$ 36 knots	$\Delta = 0.02R$ 36 knots	$\Delta = 0.02R$ 28 knots	$\Delta = 0.02R$ 20 knots
X.1	0.2725	0.2734	0.2749	0.2767
X.2	0.2716	0.2726	0.2745	0.2776
X.3	0.2716	0.2724	0.2739	0.2765
X.4	0.2720	0.2729	0.2747	0.2773
X.0	0.2721	0.2731	0.2747	0.2774
Y.1	0.2809	0.2809	0.2814	0.2808
Y.2	0.2802	0.2802	0.2811	0.2802
Y.3	0.2787	0.2789	0.2807	0.2802
Y.0	0.2793	0.2794	0.2806	0.2802

NOTES.—The results given are depths (expressed as fractions of the solar radius). Frequency sets labelled X.n and Y.n refer to unknown Models X and Y (cf. Tables 1 and 2). The actual depths at which the bases of the convection zones of Models X and Y are located are $0.2712R$ and $0.2793R$ respectively.

TABLE 6.

RESULTS FOR THE SUN

Inversion method	Inferred depth d_b/R	Inferred sound speed c_b ($10^7 \mathrm{cm\,s^{-1}}$)
Absolute	0.279	2.19
Differential, 20 knots, $\Delta = 0.02R$	0.2878	2.239
Differential, 28 knots, $\Delta = 0.02R$	0.2870	2.235
Differential, 36 knots, $\Delta = 0.02R$	0.2870	2.234
Differential, 36 knots, $\Delta = 0.01R$	0.2869	2.233

NOTE.—The table gives the depth d_b of the solar convection zone, and the sound speed c_b at this depth, as inferred by the techniques presented in this paper from the combined data set of Duvall *et al.* (1988) and Libbrecht and Kaufman (1988).

REFERENCES.

Anders, E. and Grevesse, N., 1989, *Geochim. Cosmochim. Acta*, **53**, 197.

Ando, H. and Osaki, Y., 1975, *Publ. Astron. Soc. Japan*, **27**, 581.

Baglin, A., Morel, P. J. and Schatzman, E., 1985, *Astr. Ap.*, **149**, 309.

Bahcall, J. N. and Ulrich, R. K., 1988, *Rev. Mod. Phys.*, **60**, 297.

Balmforth, N. J. and Gough, D. O., 1990, *Solar Phys.*, in the press.

Berthomieu, G., Cooper, A. J., Gough, D. O., Osaki, Y., Provost, J. and Rocca, A., 1980, in *Lecture Notes in Physics*, Vol. **125**, ed. H. A. Hill and W. Dziembowski (Berlin: Springer-Verlag), p. 307.

Boesgaard, A. M. and Steigman, G., 1985, *Ann. Rev. Astr. Ap.*, **23**, 319.

Brodsky, M.A. and Vorontsov, S.V. 1987, *Pis'ma Astr. Zh.*, **13**, 438. [English translation: *Sov. Astr. Lett.* **13**, 179].

Christensen-Dalsgaard, J., 1982, *M.N.R.A.S.*, **199**, 735.

Christensen-Dalsgaard, J., 1986, in *Seismology of the Sun and the distant Stars*, ed. D. O. Gough (Dordrecht: Reidel), p. 23.

Christensen-Dalsgaard, J., 1988, in *Seismology of the Sun and Sun-like Stars*, ed. V. Domingo and E. J. Rolfe (Noordwijk: ESA SP-286, ESTEC), p. 431.

Christensen-Dalsgaard, J., Duvall, T. L., Gough, D. O., Harvey, J. W. and Rhodes, E. J., 1985, *Nature*, **315**, 378.

Christensen-Dalsgaard, J., Däppen, W. and Lebreton, Y., 1988, *Nature*, **336**, 634.

Christensen-Dalsgaard, J., Gough, D. O. and Thompson, M. J., 1988, in *Seismology of the Sun and Sun-like Stars*, ed. V. Domingo and E. J. Rolfe (Noordwijk: ESA SP-286, ESTEC), p. 493.

Christensen-Dalsgaard, J., Gough, D. O. and Thompson, M. J., 1989, *M.N.R.A.S.*, **238**, 481.

Christensen-Dalsgaard, J., Schou, J. and Thompson, M. J., 1990, *M.N.R.A.S.*, in the press.

Cox, A. N. and Tabor, J. E., 1976, *Ap. J. Suppl.*, **31**, 271.

Cox, A. N., Guzik, J. A. and Kidman, R. B., 1989, *Ap. J.*, **342**, 1187.

Craig, I. J. D. and Brown, J. C., 1986, *Inverse problems in astronomy: a guide to inversion strategies for remotely sensed data* (Bristol: Adam Hilger).

DeLuca, E. E. and Gilman, P. A., 1986, *Geophys. Astrophys. Fluid Dyn.*, **37**, 85.

Deubner, F.-L., 1975, *Astr. Ap.*, **44**, 371.

Duvall, T. L., Harvey, J. W., Libbrecht, K. G., Popp, B. D. and Pomerantz, M. A., 1988, *Ap. J.*, **324**, 1158.

Dziembowski, W. A. and Goode, P. R., 1989, *Ap. J.*, **347**, 540.

Däppen, W. and Gough, D. O., 1984, in *Theoretical Problems in Stellar Stability and Oscillations* (Liège: Institut d'Astrophysique, Liège), p. 264.

Däppen, W., Gough, D. O. and Thompson, M. J., 1988, in *Seismology of the Sun and Sun-like Stars*, ed. V. Domingo and E. J. Rolfe (Noordwijk: ESA SP-286, ESTEC), p. 505.

Däppen, W., Mihalas, D., Hummer, D. G. and Mihalas, B. W., 1988, *Ap. J.*, **332**, 261.

Eggleton, P. P., Faulkner, J. and Flannery, B. P., 1973, *Astr. Ap.*, **23**, 325.

Faulkner, J., Gough, D. O. and Vahia, M. N., 1986, *Nature*, **321**, 226.

Fowler, W. A., Caughlan, G. R. and Zimmerman, B. A., 1975, *Ann. Rev. Astr. Ap.*, **13**, 69.

Gabriel, M., Noels, A. and Scuflaire, R., 1984, *Mem. Soc. astr. Ital.*, **55**, 169.

Gilman, P. A. and Miller, J., 1986, *Ap. J. Suppl.*, **61**, 585.

Gough, D. O., 1977, in *Proc. IAU Colloq. No. 36*, ed. R. M. Bonnet and P. Delache (Clermont-Ferrand: G. de Bussac), p. 3.

Gough, D. O., 1984, *Mem. Soc. Astron. Ital.*, **55**, 13.

Gough, D. O., 1986, in *Seismology of the Sun and the distant Stars*, ed. D. O. Gough (Dordrecht: Reidel), p. 125.

Gough, D. O. and Thompson, M. J., 1990, in *Solar interior and atmosphere*, ed. A. N. Cox, W. C. Livingston and M. Matthews (Tucson: Space Science Series, University of Arizona Press), in the press.

Gough, D. O. and Weiss, N. O., 1976, *M.N.R.A.S.*, **176**, 589.

Huebner, W. F., Merts, A. L., Magee, N. H. and Argo, M. F., 1977, *Astrophysical Opacity Library*, Los Alamos Scientific Laboratory report LA-6760-M.

Hummer, D. G. and Mihalas, D., 1988, *Ap. J.*, **331**, 794.

Korzennik, S. G. and Ulrich, R. K., 1989, *Ap. J.*, **339**, 1144.

Kosovichev, A.G. 1988, in *Seismology of the Sun and Sun-like Stars*, ed. V. Domingo and E. J. Rolfe (Noordwijk: ESA SP-286, ESTEC), p. 553.

Lebreton, Y. and Maeder, A., 1987, *Astr. Ap.*, **175**, 99.

Libbrecht, K. G. and Kaufman, J. M., 1988, *Ap. J.*, **324**, 1172.

Lubow, S. H., Rhodes, E. J. and Ulrich, R. K., 1980, in *Lecture Notes in Physics*, Vol. **125**, ed. H. A. Hill and W. Dziembowski (Berlin: Springer-Verlag), p. 300.

Mihalas, D., Däppen, W. and Hummer, D. G., 1988, *Ap. J.*, **331**, 815.

Noerdlinger, P. D., 1977, *Astr. Ap.*, **57**, 407.

Pagel, B. E. J., 1989, in *Evolutionary Phenomena in Galaxies*, ed. J. Beckman and B. E. J. Pagel (Cambridge: Cambridge University Press).

Parker, E. N., 1975, *Ap. J.*, **198**, 205.

Parker, E. N., 1987, *Solar Phys.*, **110**, 11.

Parker, P. D., 1986, in *Physics of the Sun*, Vol. 1, ed. P. A. Sturrock, T. E. Holzer, D. Mihalas and R. K. Ulrich (Dordrecht: Reidel), p. 15.

Pidatella, R. M. and Stix, M., 1986, *Astr. Ap.*, **157**, 338.

Provost, J., 1984, *Proc. IAU Symposium No 105: "Observational Tests of Stellar Evolution Theory"*, ed. A. Maeder and A. Renzini (Dordrecht: Reidel), p. 47.

Rhodes, E. J., Ulrich, R. K. and Simon, G. W., 1977, *Ap. J.*, **218**, 901.

Rolfs, C. and Kavanagh, R. W., 1986, *Nucl. Phys.*, **A455**, 179.

Roxburgh, I. W., 1985, *Solar Phys* ., **100**, 21.

Schatzman, E., Maeder, A., Angrand, F. and Glowinski, R., 1981, *Astr. Ap.*, **96**, 1.

Schmitt, J. H. M. M., Rosner, R. and Bohn, H. U., 1984, *Ap. J.*, **282**, 316.

Shibahashi, H. and Sekii, T. 1988, in *Seismology of the Sun and Sun-like Stars*, ed. V. Domingo and E. J. Rolfe (Noordwijk: ESA SP-286, ESTEC), p. 471.

Thompson, M. J., 1988, in *Seismology of the Sun and Sun-like Stars*, ed. V. Domingo and E. J. Rolfe (Noordwijk: ESA SP-286, ESTEC), p. 321.

Turck-Chièze, S., Cahen, S., Cassé, M. and Doom, C., 1988, *Ap. J.*, **335**, 415.

Ulrich, R. K. and Rhodes, E. J., 1977, *Ap. J.*, **218**, 521.

van Ballegooijen, A. A., 1982, *Astr. Ap.*, **113**, 99.

Vorontsov, S. V., 1988, in *Seismology of the Sun and Sun-like Stars*, ed. V. Domingo and E. J. Rolfe (Noordwijk: ESA SP-286, ESTEC), p. 475.

Vorontsov, S. V. and Zharkov, V. N., 1989, *Sov. Sci. Rev. E. Ap. Space Phys.*, **7**, 1.

Wambsganss, J., 1988, *Astr. Ap.*, **205**, 125.

FIGURE CAPTIONS:

Figure 1. The sound speed in the Sun as inferred by Christensen-Dalsgaard *et al.* (1985) (solid curve); the dashed curve shows the sound speed in a standard solar model for comparison. The inset shows in greater detail the inferred sound speed near the base of the convection zone.

Figure 2. The particular error realization added into the frequency set X.1 for testing the inversion procedures. In addition to the much greater spread for shallowly penetrating modes, note the systematic error introduced for modes of degree $l > 120$.

Figure 3. (a) The exact sound-speed difference between Model X and reference model 10 of Table 4 (dashed line), in the sense Model X minus reference model. The solid line shows the sound-speed difference after it has been artificially smoothed according to equations (5.1) – (5.3), with $d = 0.07R$. The convection zone in Model X is shallower than that in the reference model; this causes the negative excursion in δc just beneath the base of the convection zone in Model X. (b) Corresponding to (a), this panel shows (solid curve) the function W estimated for Model X by using $(1 + \delta c/c)c(r)$ as the sound speed in definition (1.4), where $c(r)$ is the exact sound speed in the reference model and $\delta c/c$ is the artificially smoothed sound-speed difference shown as a solid curve in (a). Also shown are the exact functions W for Model X (dot-dash line) and the reference model (regular dashed line). (c) As (a) but using reference model 6 of Table 4. The convection zones in Model X and the reference model have similar depths. (d) As (b) but corresponding to the reference model used in panel (c). (e) As (a) but using reference model 5 of Table 4. In this case the convection zone of Model X is slightly deeper than that in the reference model. (f) As (b) but corresponding to the reference model used in panel (e).

Figure 4. The quantity $\overline{\delta W}$ computed from the artificially smoothed sound speed differences between Model X and (from left to right) reference models 5, 6, 7 and 8 of Table 4, plotted against the depths of the convection zones in the reference models. The value of Δ was $0.02R$. The artificial smoothing parameter d took the values $0.07R$ (plus signs), $0.05R$ (stars) and zero (crosses). From a linear fit to each of these three cases one would infer that $\overline{\delta W}$ is zero at $d_b = 0.2771R$, $0.2749R$ and $0.2722R$ respectively. The exact depth d_b of Model X's convection zone is $0.2712R$.

Figure 5. (a) The exact sound-speed difference between Model X and reference model 10 of Table 4 (dashed line), in the sense Model X minus reference model, together with the sound-speed difference inferred by differential inversion using 28 (dot-dash line) or 36 (solid line) w-spline knots. (b) Corresponding to (a), this panel shows the function W estimated for Model X by using the sound-speed difference from the 28-knot inversion (dot-dash line) and the 36-knot inversion (solid line). Also shown is the exact function W for the reference model (regular dashed line). (The exact W for Model X can be seen in Figure 3b.) (c) As (a) but using reference model 6 of Table 4. (d) As (b) but corresponding to the reference model used in panel (c). (e) As (a) but using reference model 5 of Table 4. (f) As (b) but corresponding to the reference model used in panel (e).

Figure 6. The quantity $\overline{\delta W}$ computed from the estimated sound-speed differences between Model X and the reference models in Table 4, plotted against the depths of the convection zones in the reference models. The results were obtained from differential inversions using 36 w-spline knots, and the value of parameter Δ was $0.01R$. Data points for models based on the LAOL opacities are indicated by stars, those for models based on the CT opacities are shown with crosses.

Figure 7. (a) The inferred sound-speed difference $\delta c/c$ between Model X and model 6 of Table 4, in the sense Model X minus reference model (solid line), together with the exact sound-speed difference

(dashed line). Thirty-six w-knots were used in the inversion. (b) As (a), but for Model Y and reference model 7 of Table 4.

Figure 8. (a) The coefficients d_{nl}, defined by equation (5.5), plotted against $\nu_{nl}/(l+\frac{1}{2})$. These coefficients show the weight given to any particular datum $\delta\nu/\nu$ in the estimate $\overline{\delta c/c}(r_0)$ of the relative sound-speed difference at $r = r_0$. The plotted coefficients are for $r_0 = 0.65R$, for an inversion with 36 w- and 20 ω-spline knots. Dots and crosses indicate data for $l < 100$ and $l > 100$ respectively. The upper axis shows the radius r_t of the asympototic lower turning point of the modes, i.e., the radius at which $c/r = \omega/(l+1/2)$. (b) As (a) but for $r_0 = 0.75R$. The coefficients are not purely functions of $\nu/(l+1/2)$, as they are for the asymptotic rotation inversions of, e.g., Christensen-Dalsgaard, Schou and Thompson (1990): this is because the frequency differences have an additional dependency on frequency, through the function H_2.

Figure 9. (a) Scaled frequency differences $(S(w)/\tau_0)\delta\nu/\nu$ between the Sun and reference model 13 of Table 4, plotted against ν/L. The function $S(w)$ is given by equation (2.4). The constant τ_0 is the adiabatic sound travel time along a radial path from the centre to the surface of the model; $S(w)/\tau_0 \to 1$ as $w \to \infty$. The upper axis shows the radius of the lower turning point (see Fig. 8). (b) The same scaled frequency differences after the fitted function $\overline{H}_2(\omega)$ has been removed. Also shown are the fitted spline $\overline{H}_1(w)$ (dashed line) and the positions of the spline knots (bold dots). The spline fit used 36 knots for each of the w- and ω-splines.

Figure 10. (a) The inferred sound-speed difference $\delta c/c$ between the Sun and model 13 of Table 4, in the sense Sun minus model. The results were obtained using the differential inversion method, with 20 (dot-dash line), 28 (regular dashed line) and 36 (solid line) w-knots. The reference model was adjusted to have almost the correct d_b by a suitable artificial modification to the opacity. As a result

$\delta c/c$ is very small near the base of the convection zone. The negative $\delta c/c$ at $r \simeq 0.4R$ indicates that the assumed opacity modification extends to too high a temperature. (b) The inferred function W for the 36-knot inversion of the solar data (solid curve), together with W for the reference model (dashed curve).

Figure 11. Temperature T_b at the base of the convection zones of the reference models listed in Table 4. Filled symbols represent evolutionary models, and open symbols represent static models computed with opacity adjusted as in equation (3.1) and with the hydrogen abundance and mixing-length parameter scaled in the manner described in the text such as to yield the correct solar radius and luminosity. Circles represent models computed with the MHD equation of state (Mihalas *et al.* 1988) and squares with the EFF equation of state (Eggleton *et al.* 1973). The lower sequence of models, connected by a straight line, was computed with opacities interpolated from the tables of Cox and Tabor (1976); the upper sequence used the Los Alamos Opacity Library (Huebner *et al.* 1977). The arrows indicate the direction of increasing opacity scaling factor A and increasing envelope helium abundance Y_0 in the static models. The shaded vertical band extends over the range of uncertainty in the value of d_b/R determined from the inversion of the solar p-mode frequencies.

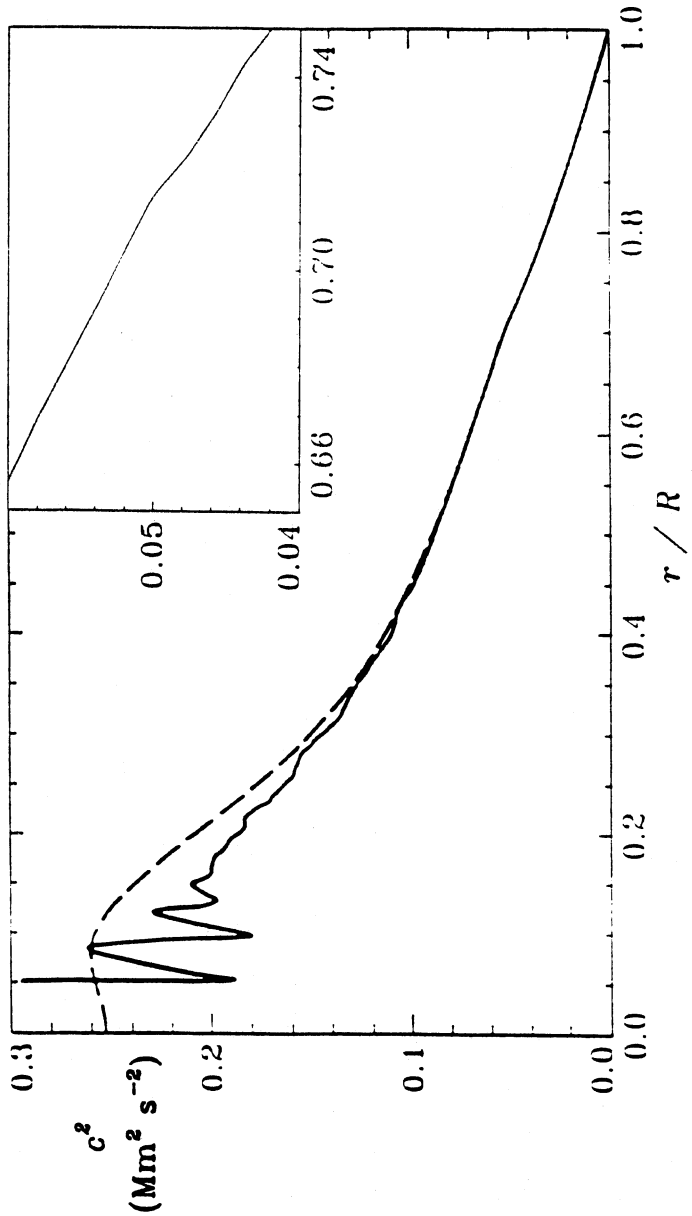

Fig. 1

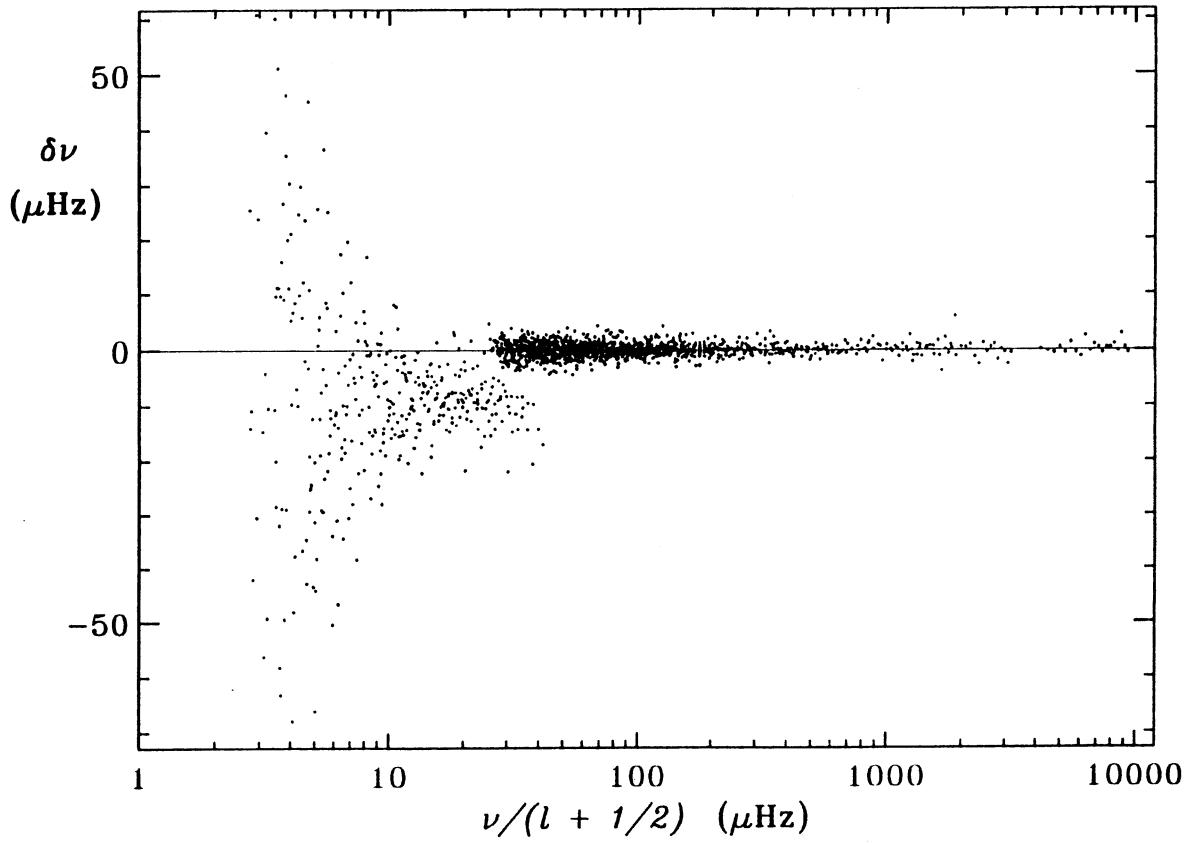
50
δν
(μHz)
0
−50
1
10
100
1000
10000
ν/(l + 1/2) (μHz)

Fig. 2

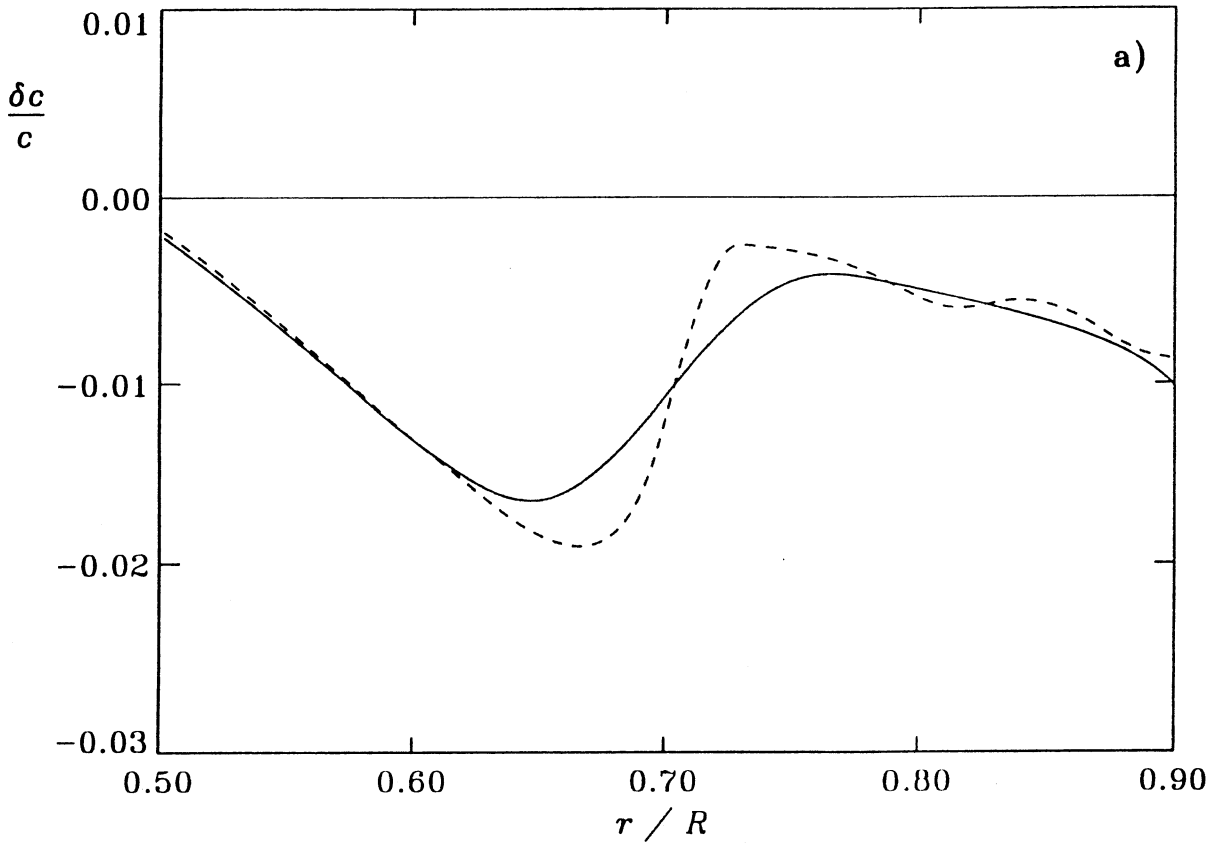
0.01
δc/c
0.00
−0.01
−0.02
−0.03
a)
0.50
0.60
0.70
0.80
0.90
r / R

Fig. 3a

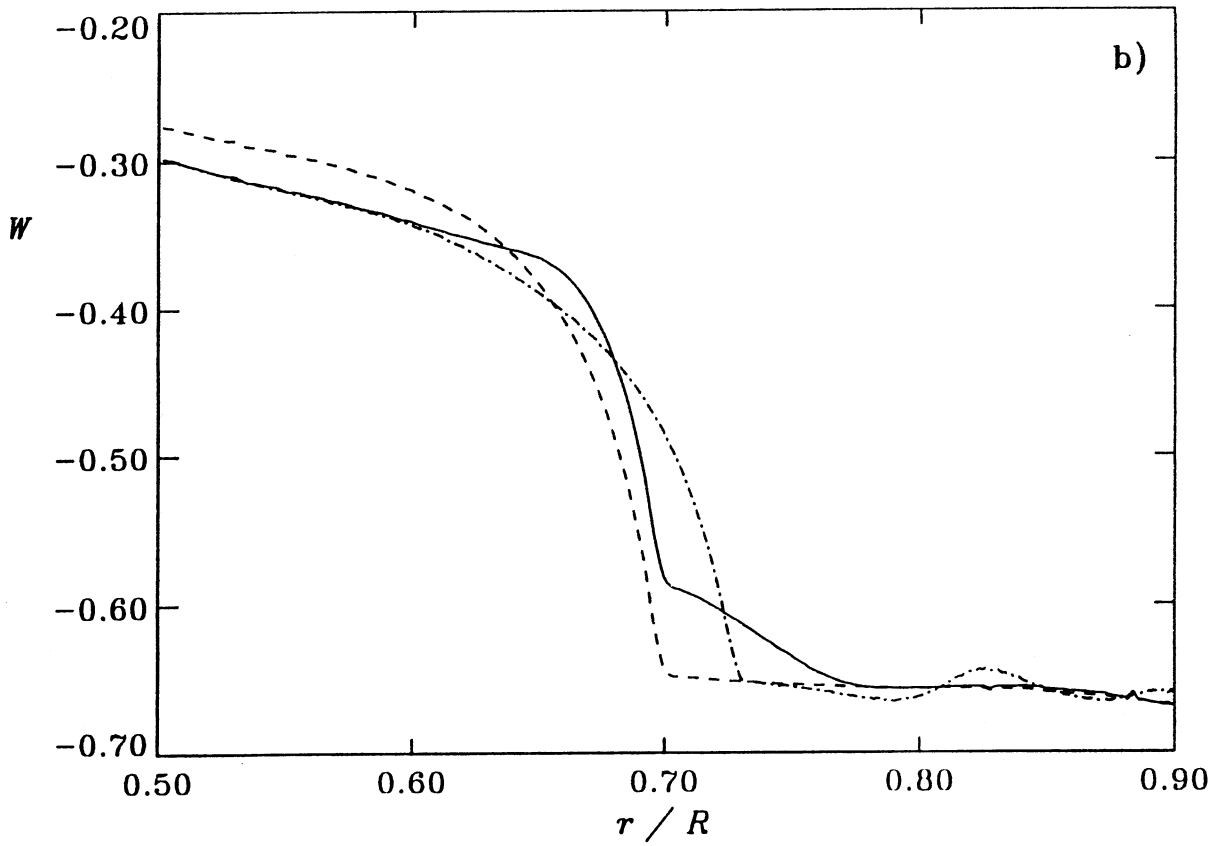
b)
W
−0.20
−0.30
−0.40
−0.50
−0.60
−0.70
0.50
0.60
0.70
0.80
0.90
r / R

Fig. 3b

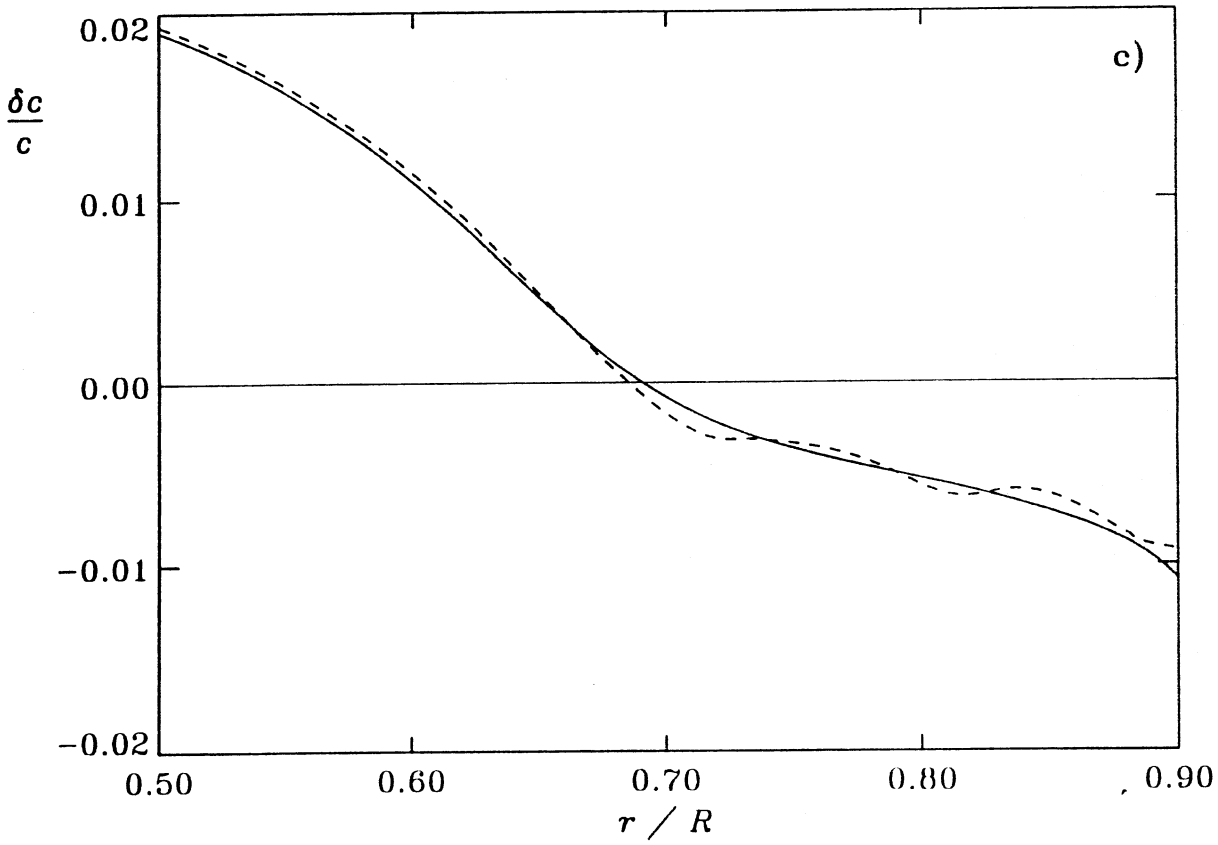
c)
δc / c
0.02
0.01
0.00
−0.01
−0.02
0.50
0.60
0.70
0.80
0.90
r / R

Fig. 3c

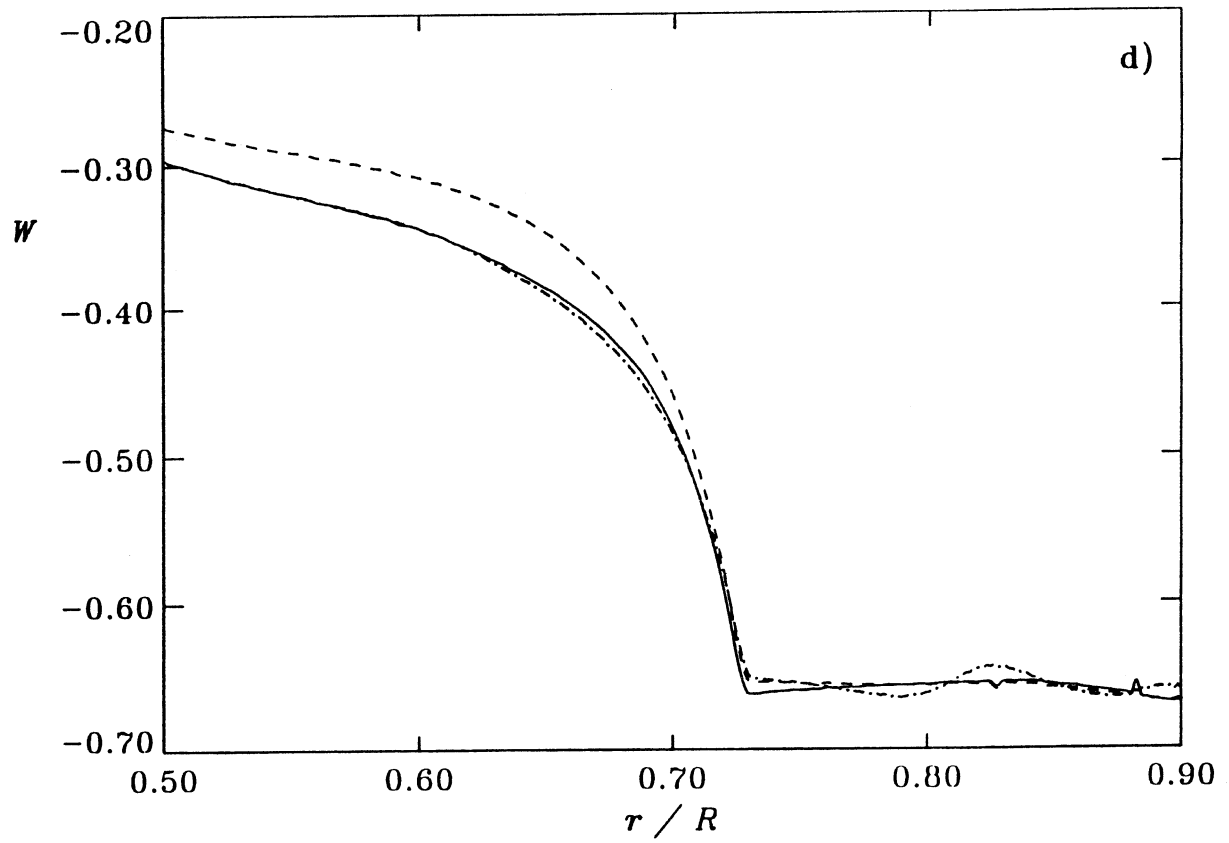
d)
−0.20
−0.30
−0.40
−0.50
−0.60
−0.70
W
0.50
0.60
0.70
0.80
0.90
r / R

Fig. 3d

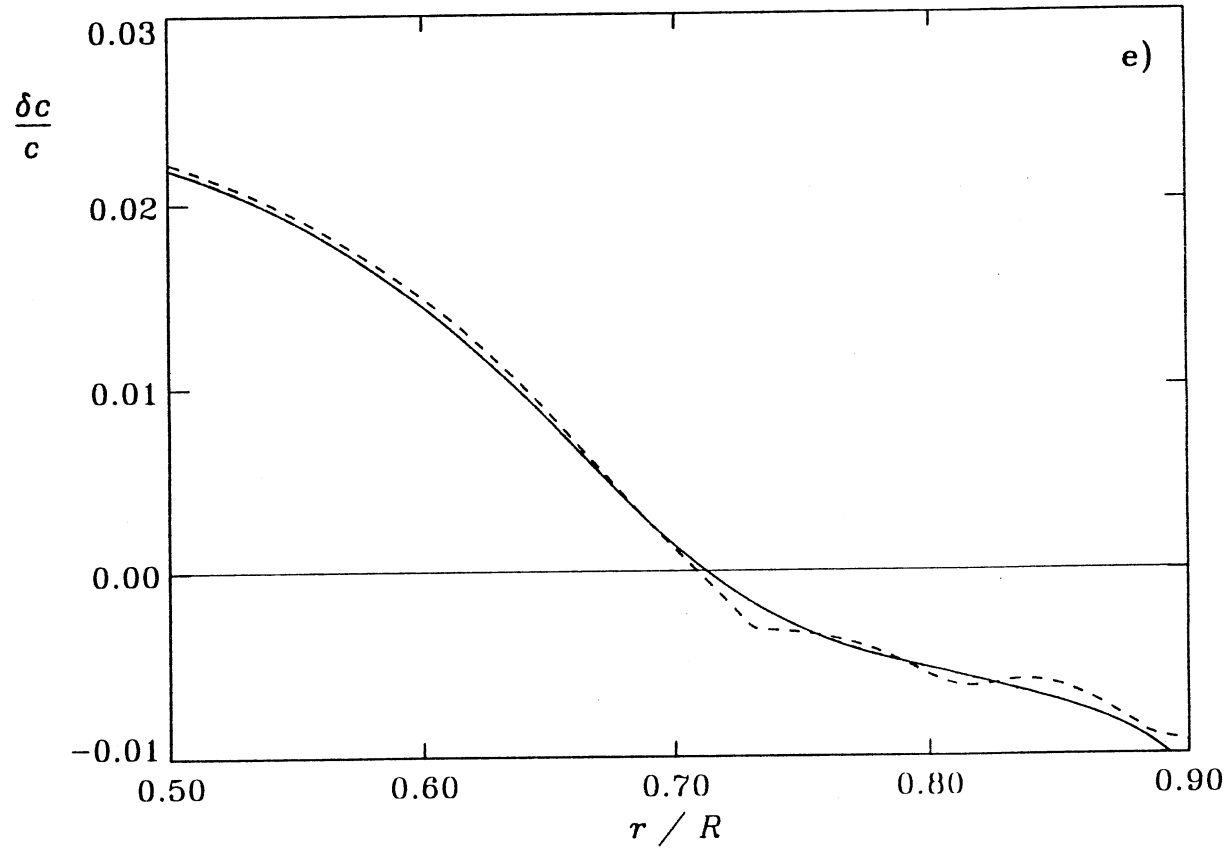
e)
0.03
0.02
0.01
0.00
−0.01
δc / c
0.50
0.60
0.70
0.80
0.90
r / R

Fig. 3e

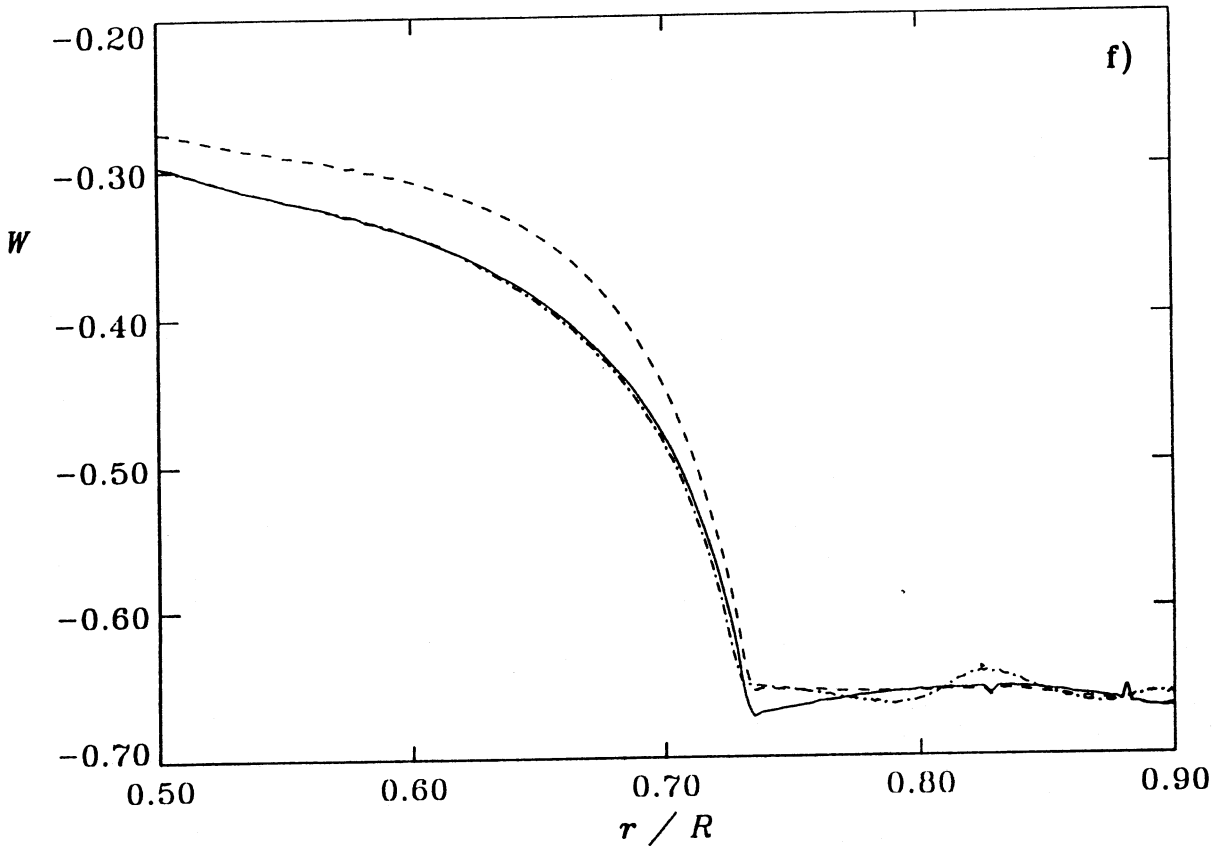
f)
W
−0.20
−0.30
−0.40
−0.50
−0.60
−0.70
0.50
0.60
0.70
0.80
0.90
r / R

Fig. 3f

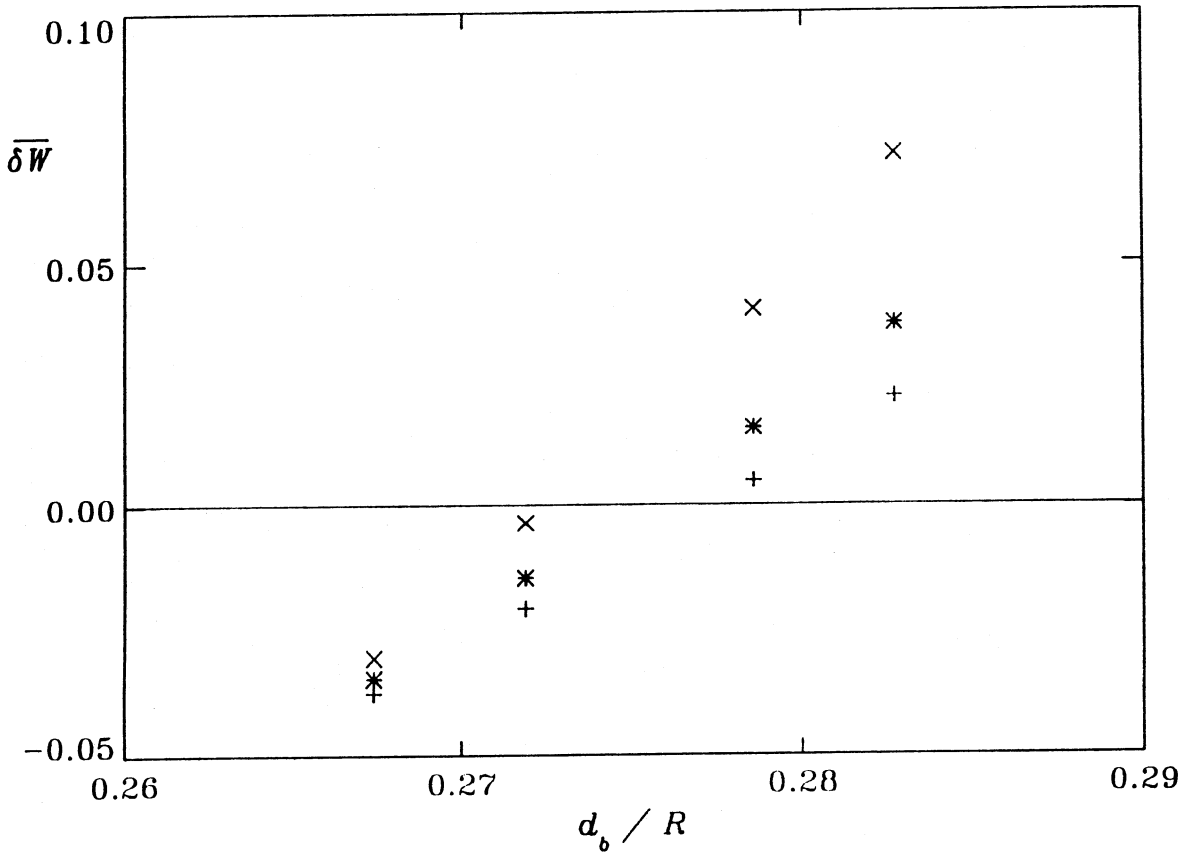
δW
0.10
0.05
0.00
−0.05
0.26
0.27
0.28
0.29
d_b / R

Fig. 4

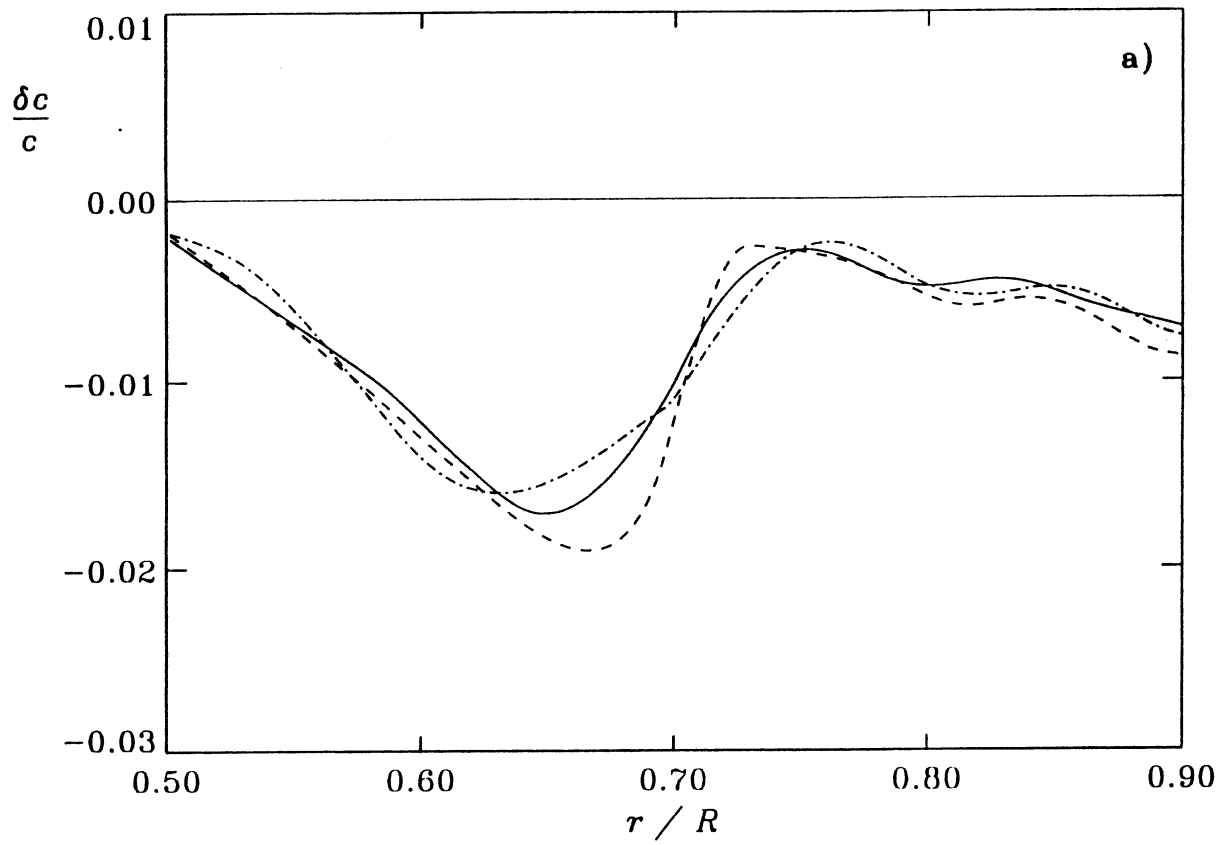
a)
$\frac{\delta c}{c}$
0.01
0.00
−0.01
−0.02
−0.03
0.50
0.60
0.70
0.80
0.90
r / R

Fig. 5a

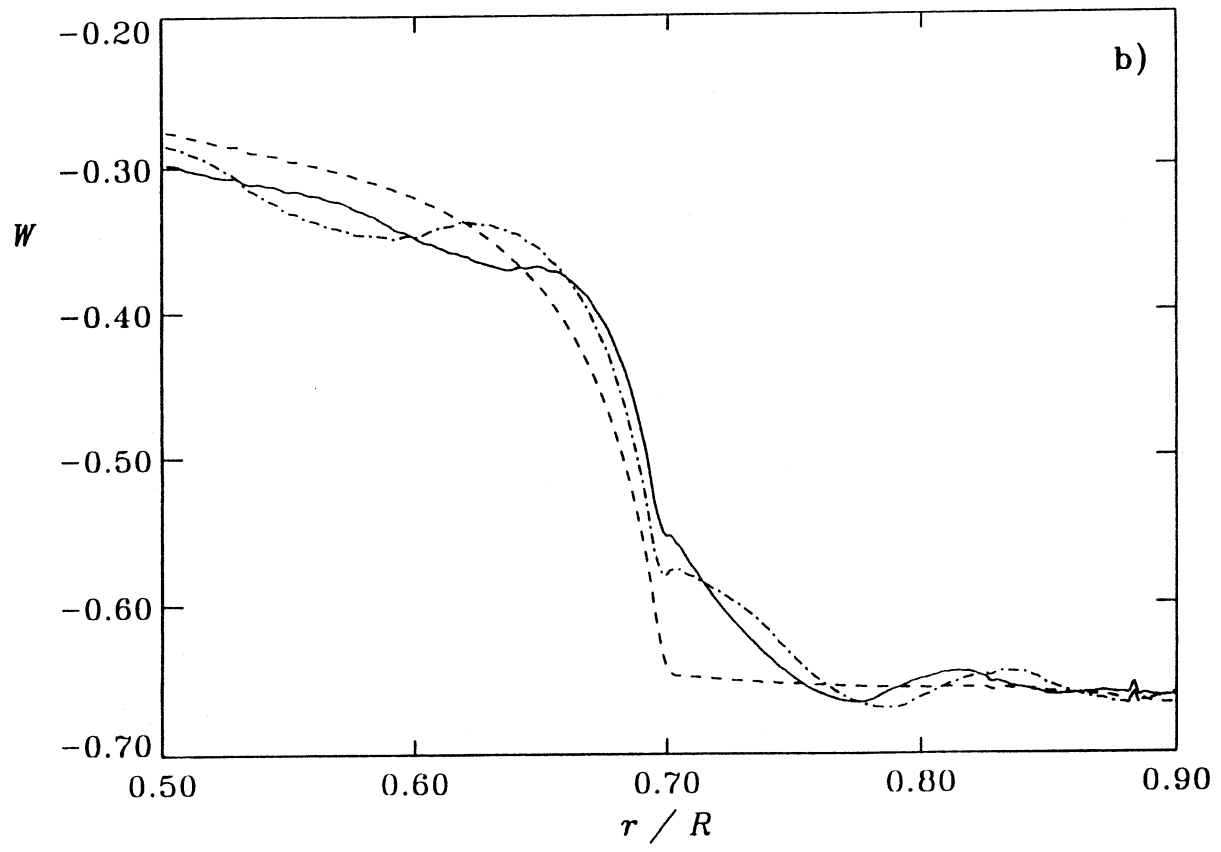
b)
W
−0.20
−0.30
−0.40
−0.50
−0.60
−0.70
0.50
0.60
0.70
0.80
0.90
r / R

Fig. 5b

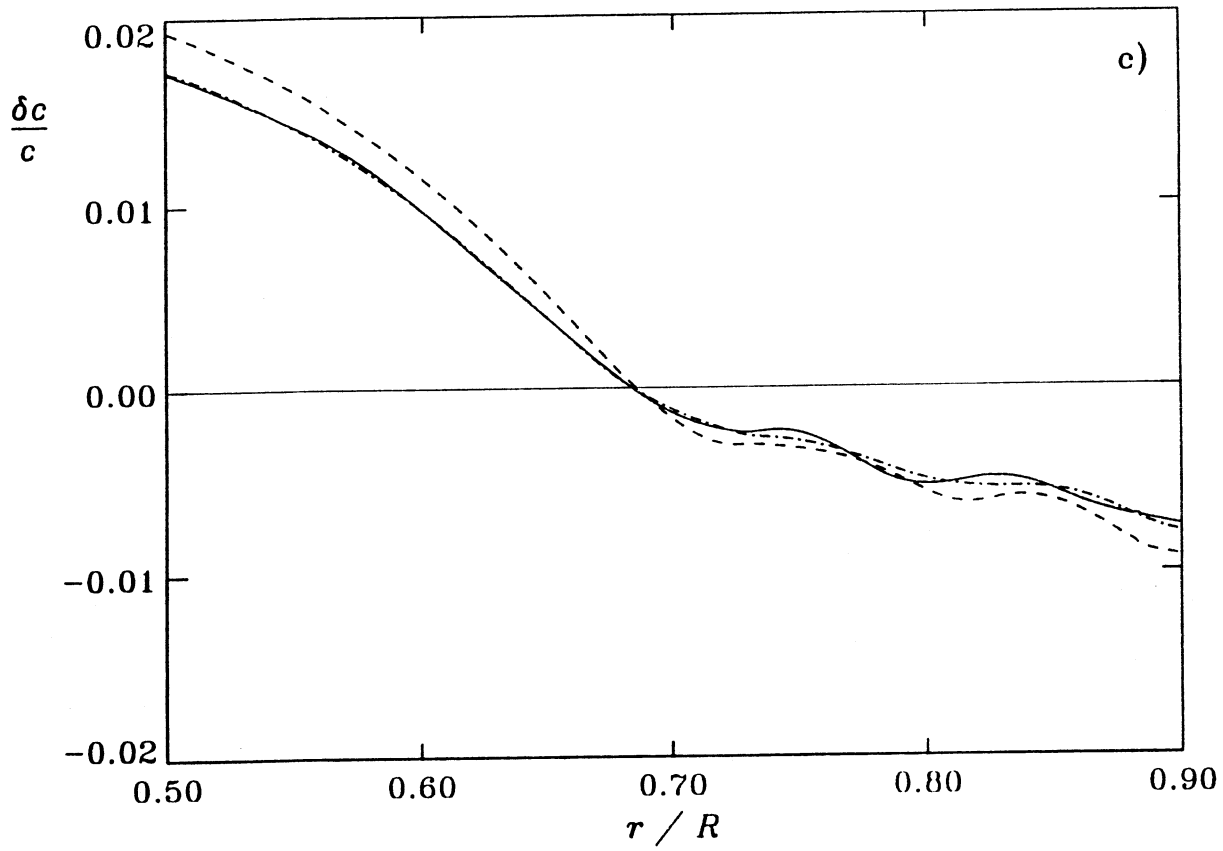
c)
δc/c
0.02
0.01
0.00
−0.01
−0.02
0.50
0.60
0.70
0.80
0.90
r / R

Fig. 5c

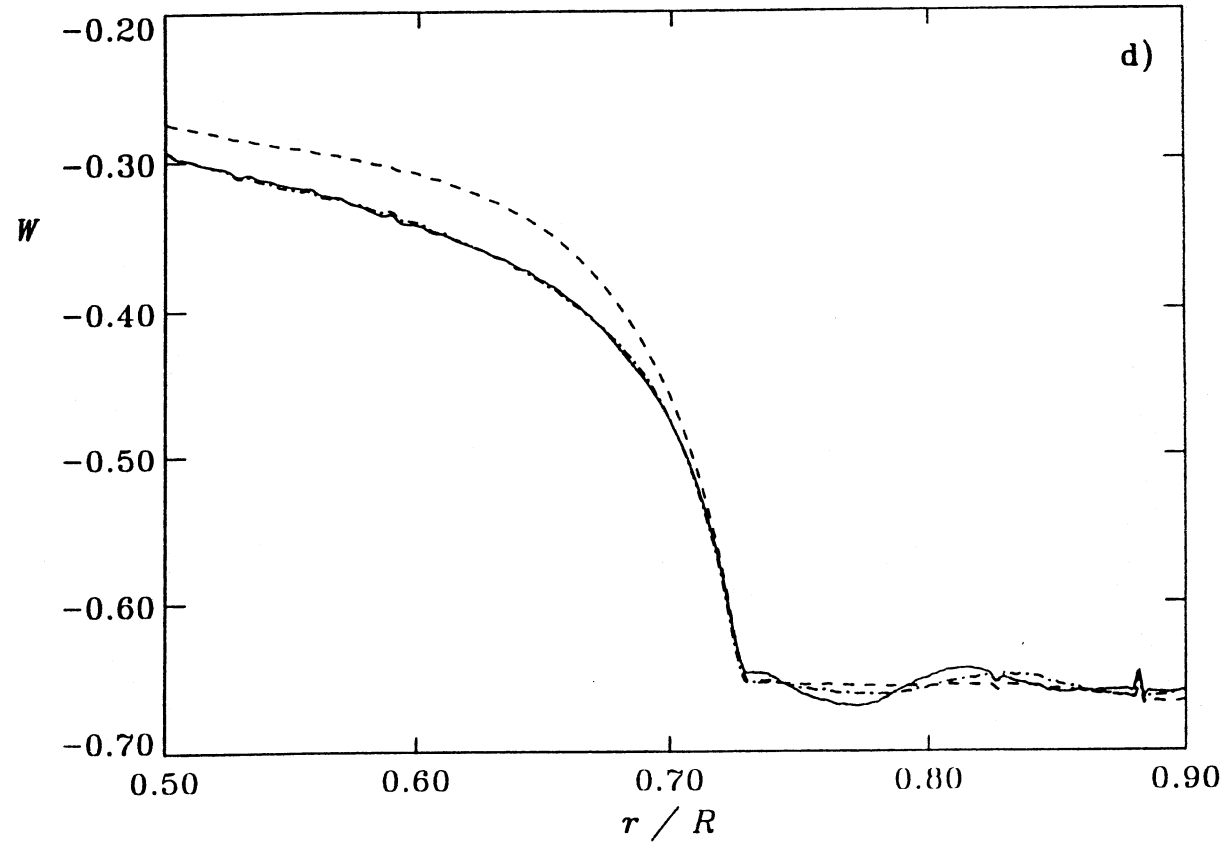
d)
W
−0.20
−0.30
−0.40
−0.50
−0.60
−0.70
0.50
0.60
0.70
0.80
0.90
r / R

Fig. 5d

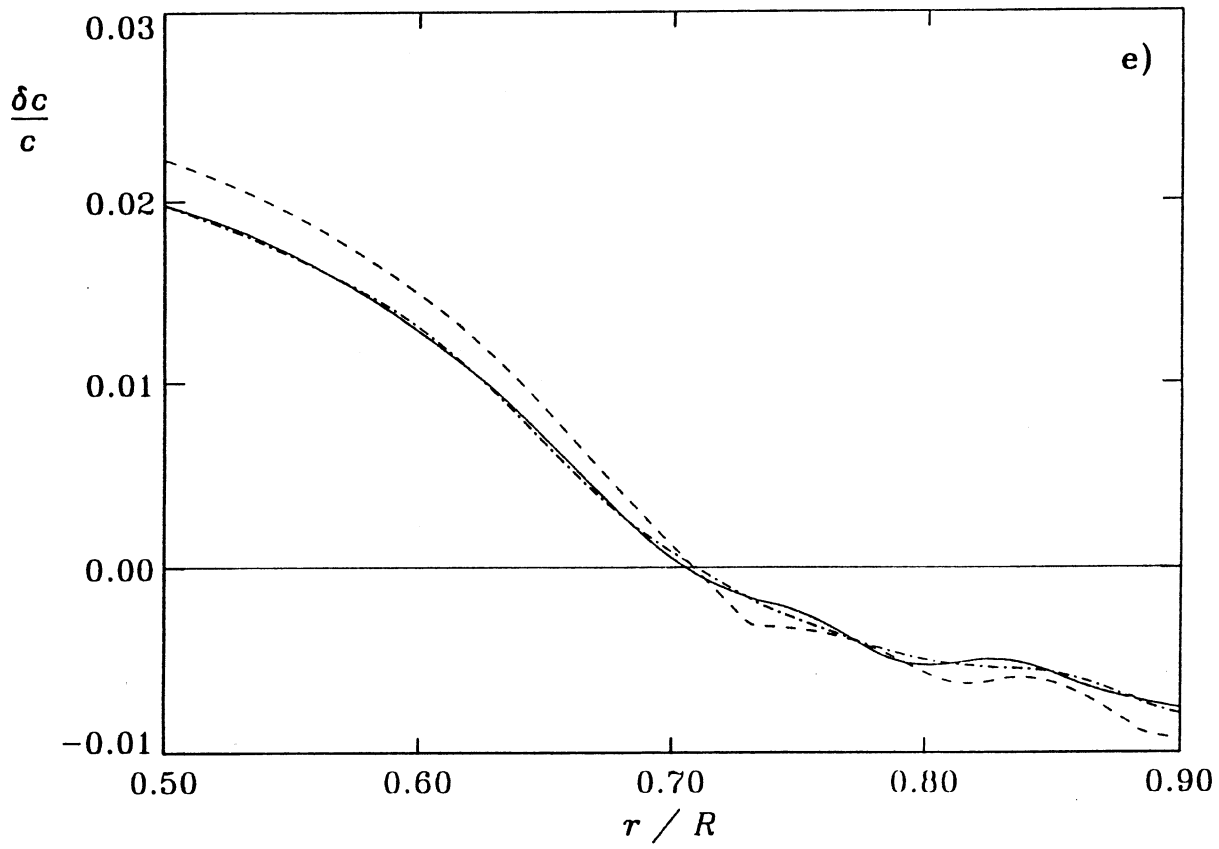
e)
δc / c
0.03
0.02
0.01
0.00
−0.01
0.50
0.60
0.70
0.80
0.90
r / R

Fig. 5e

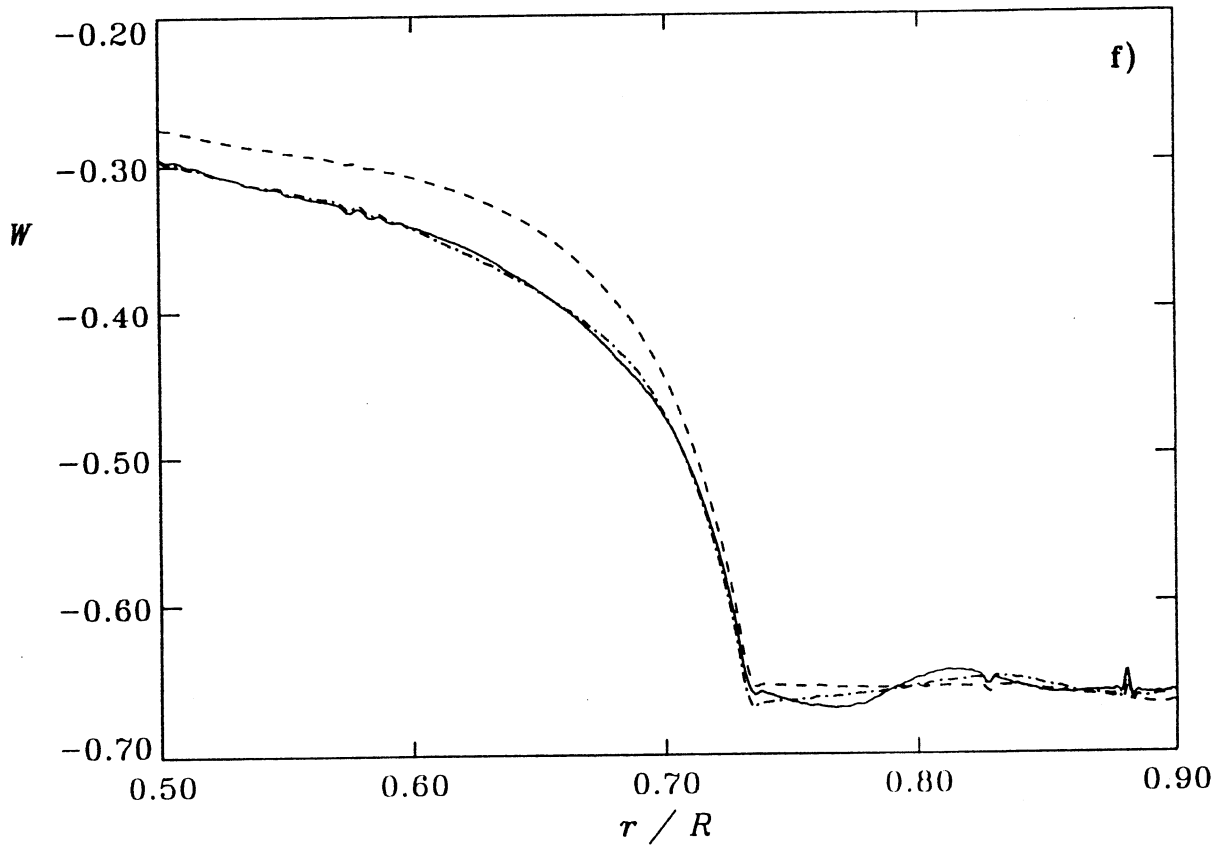
f)
W
−0.20
−0.30
−0.40
−0.50
−0.60
−0.70
0.50
0.60
0.70
0.80
0.90
r / R

Fig. 5f

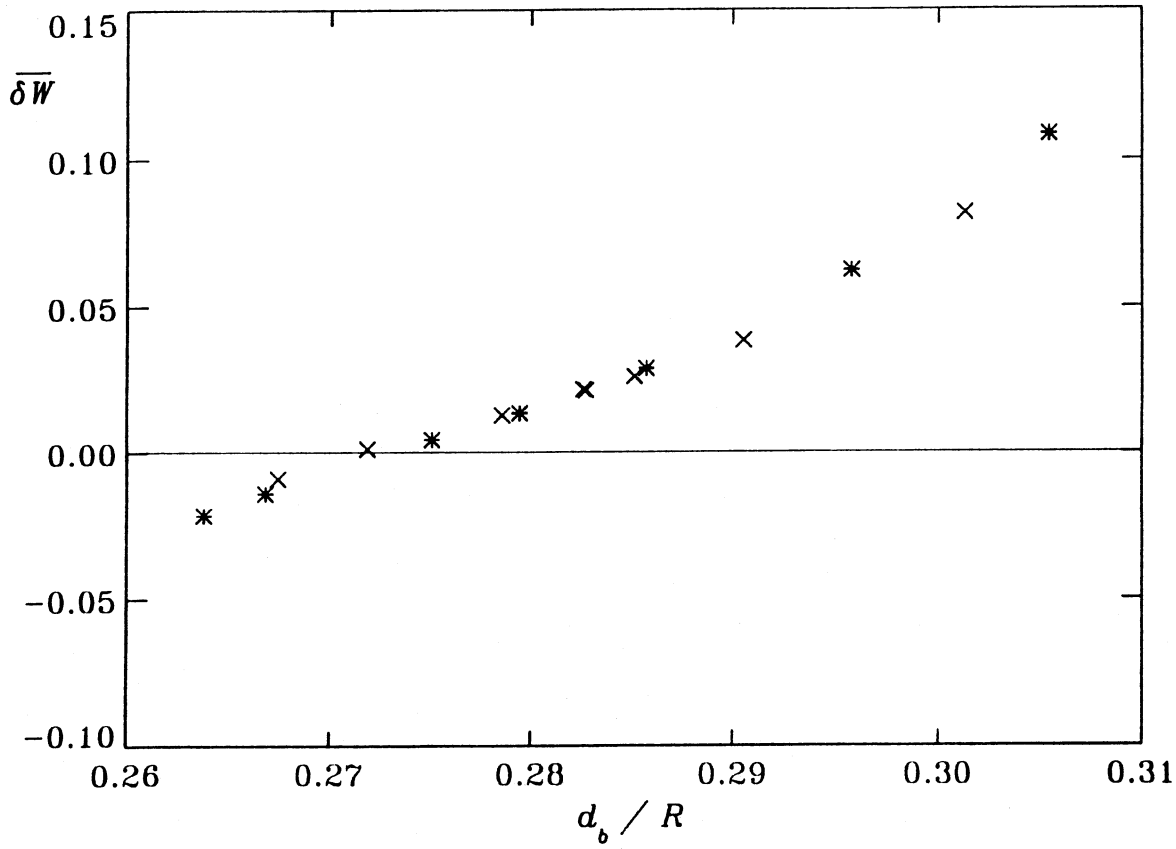
0.15
$\overline{\delta W}$
0.10
0.05
0.00
−0.05
−0.10
0.26
0.27
0.28
0.29
0.30
0.31
d_b / R

Fig. 6

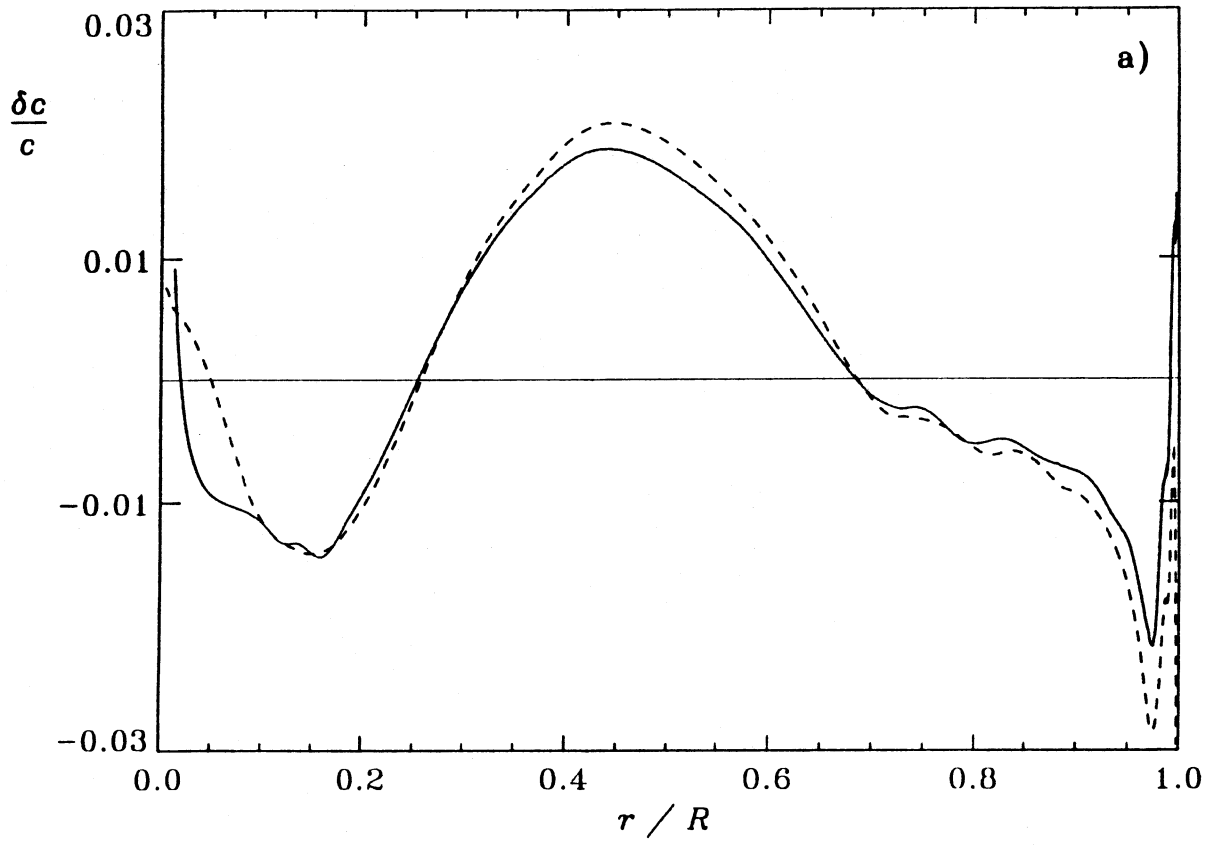
0.03
a)
$\frac{\delta c}{c}$
0.01
−0.01
−0.03
0.0
0.2
0.4
0.6
0.8
1.0
r / R

Fig. 7a

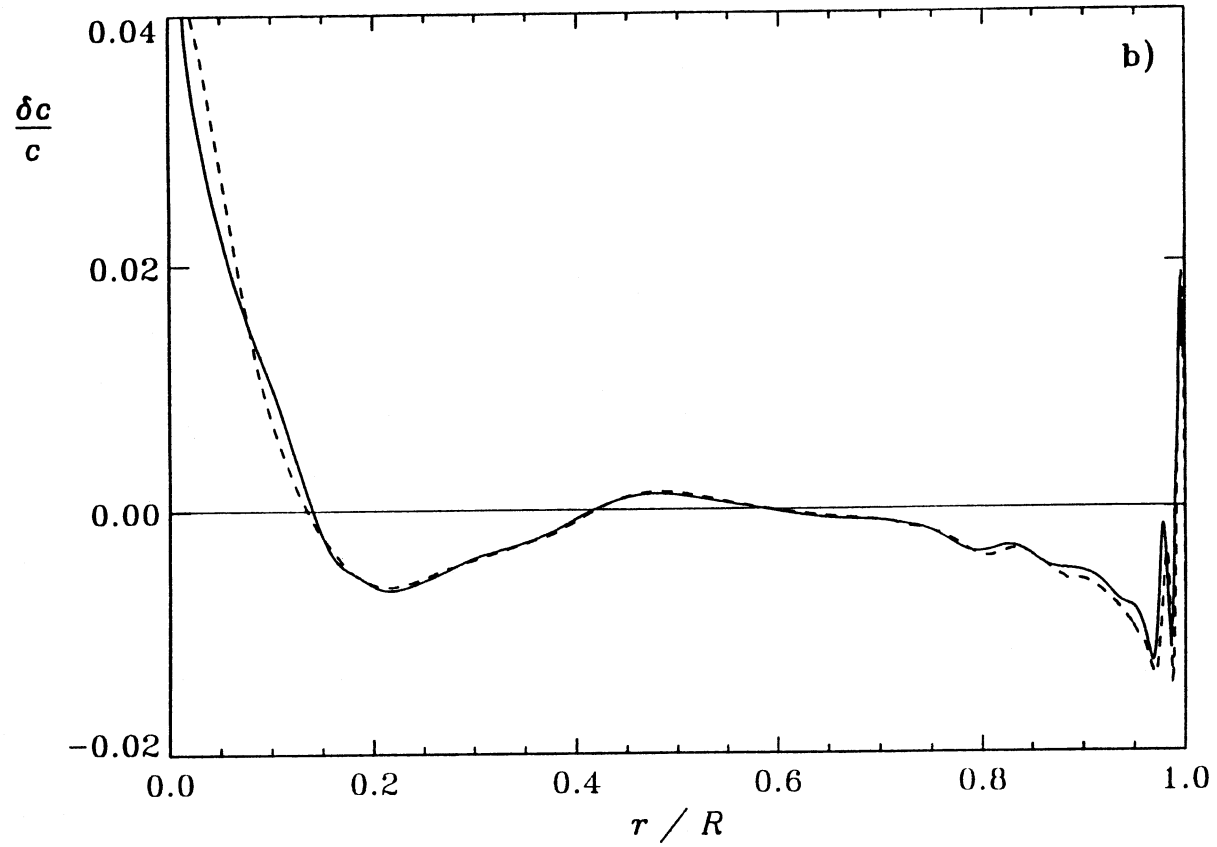
b)
δc/c
0.04
0.02
0.00
−0.02
0.0
0.2
0.4
0.6
0.8
1.0
r / R

Fig. 7b

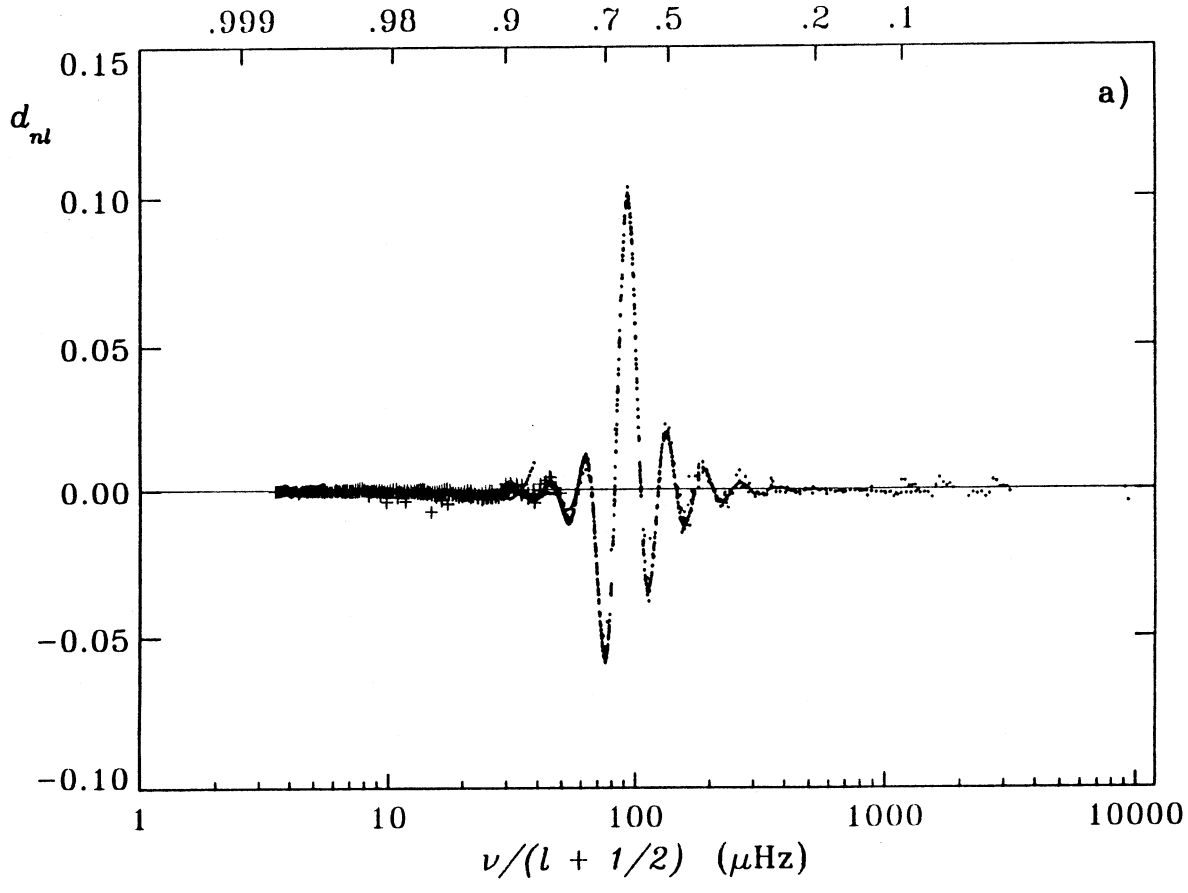
a)
.999
.98
.9
.7
.5
.2
.1
d_{nl}
0.15
0.10
0.05
0.00
−0.05
−0.10
1
10
100
1000
10000
ν/(l + 1/2) (μHz)

Fig. 8a

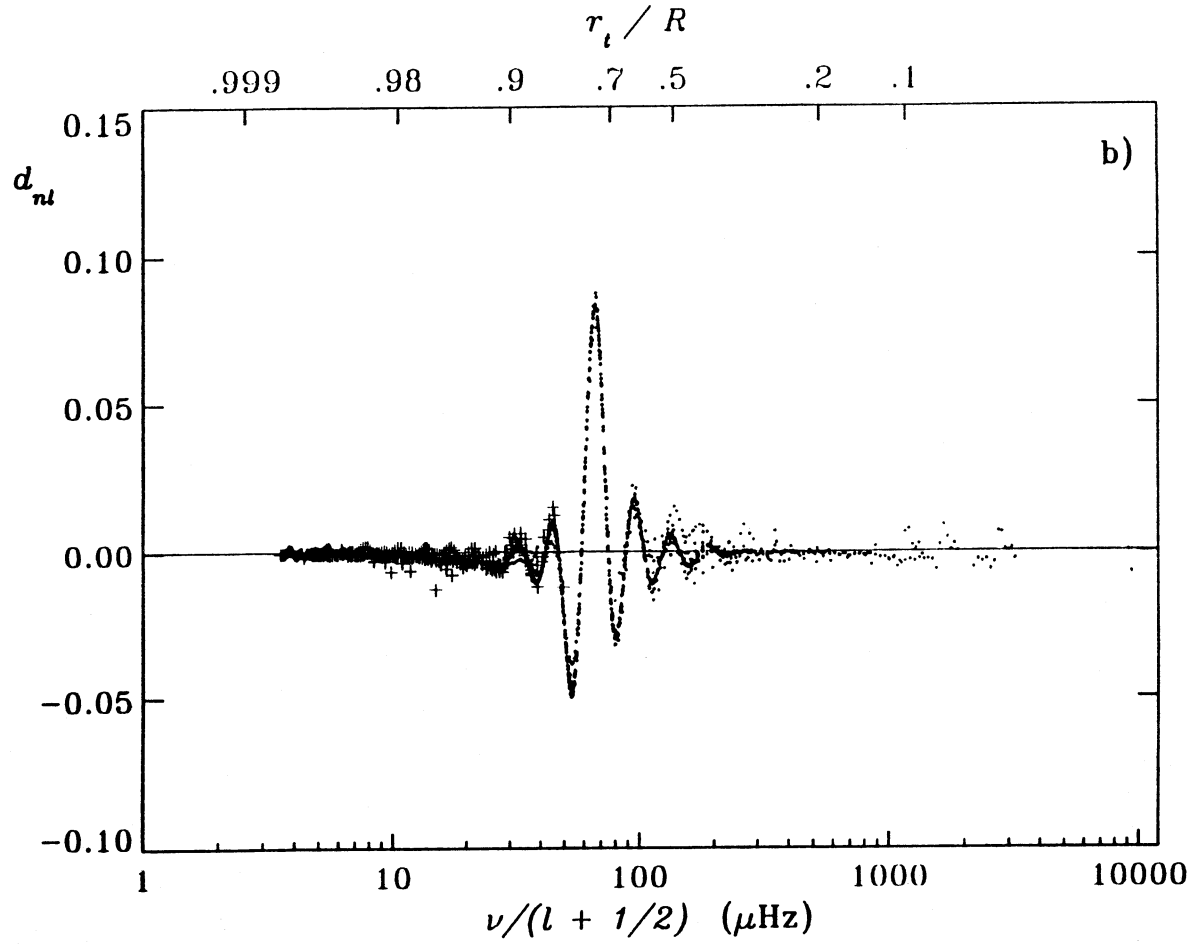
r_t / R
.999
.98
.9
.7
.5
.2
.1
b)
d_{nl}
0.15
0.10
0.05
0.00
−0.05
−0.10
1
10
100
1000
10000
$\nu/(l + 1/2)$ (μHz)

Fig. 8b

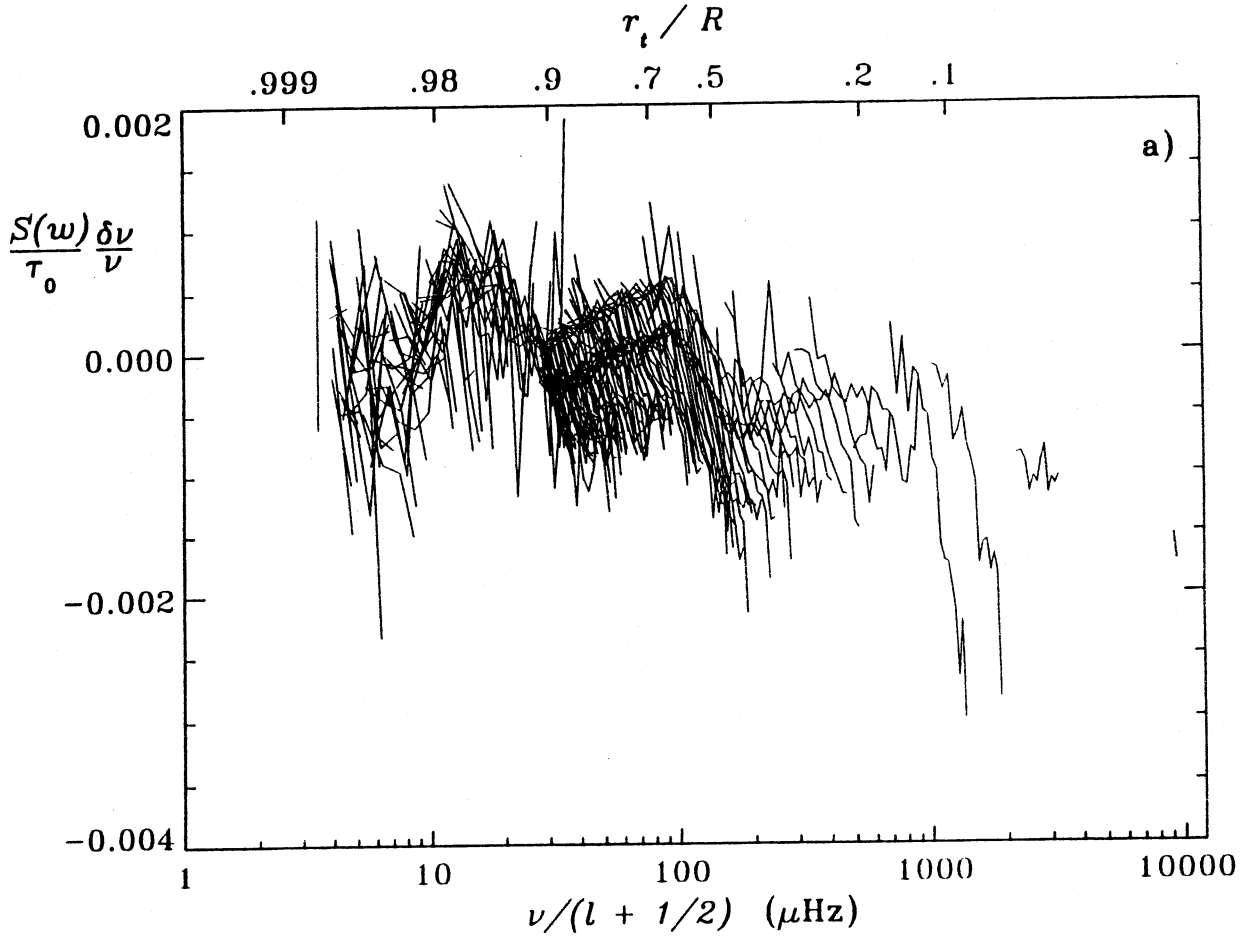
r_t / R
.999
.98
.9
.7
.5
.2
.1
a)
$\frac{S(w)}{\tau_0}\frac{\delta\nu}{\nu}$
0.002
0.000
−0.002
−0.004
1
10
100
1000
10000
$\nu/(l + 1/2)$ (μHz)

Fig. 9a

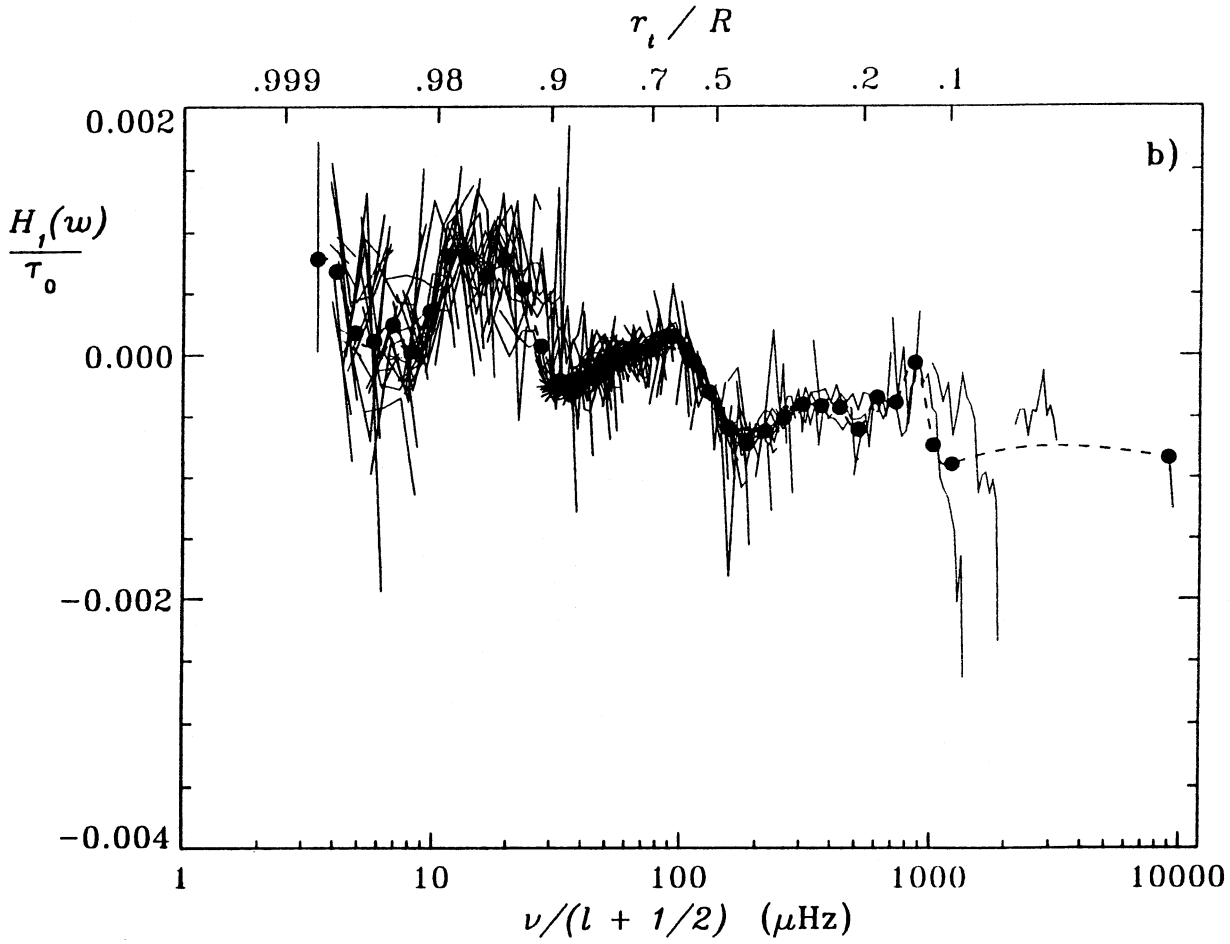

Fig. 9b

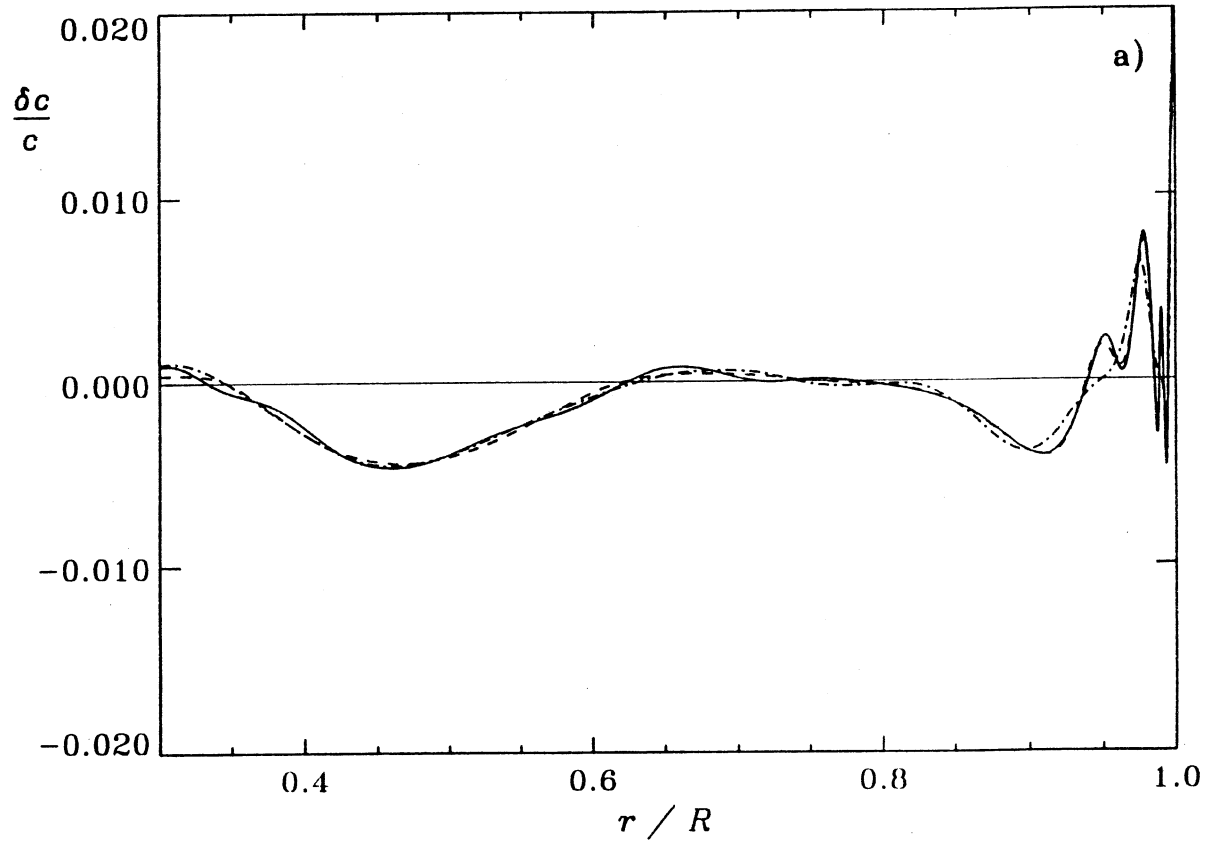

Fig. 10a

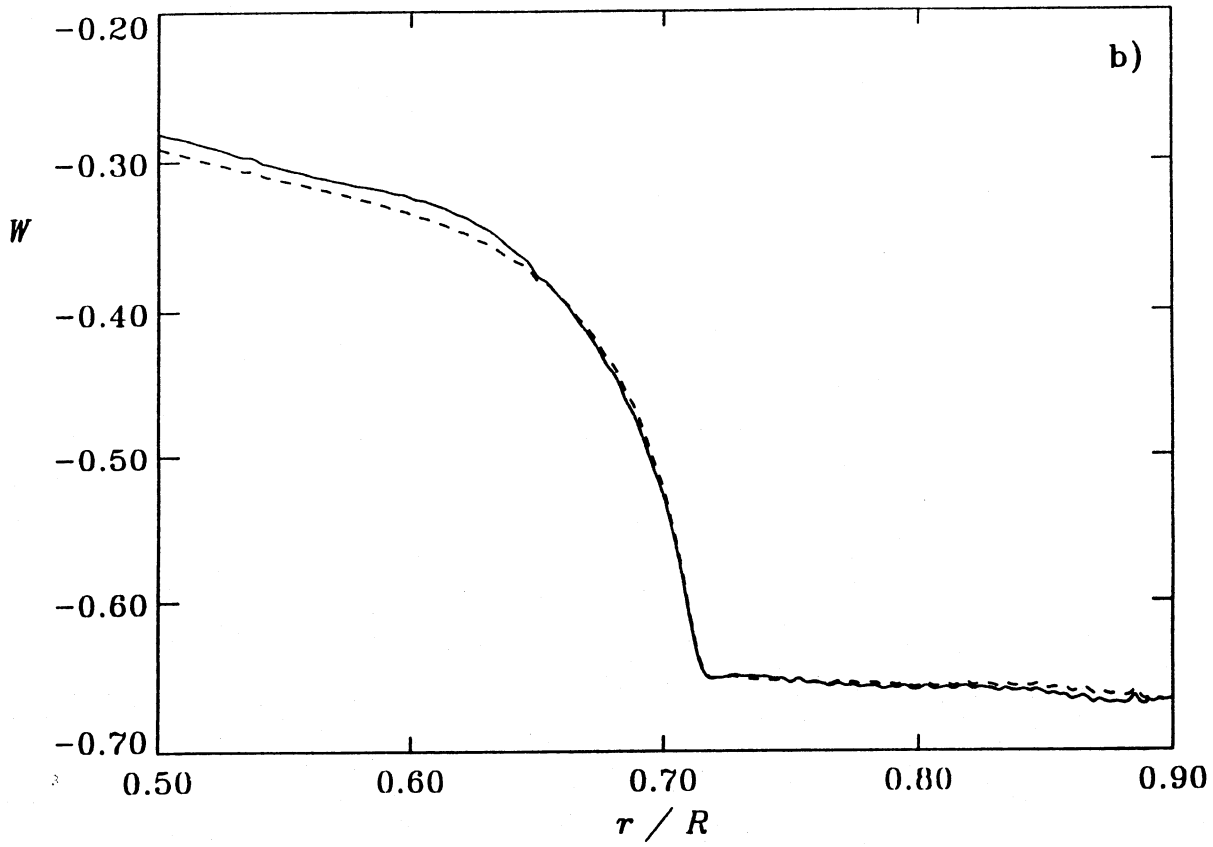

Fig. 10 b

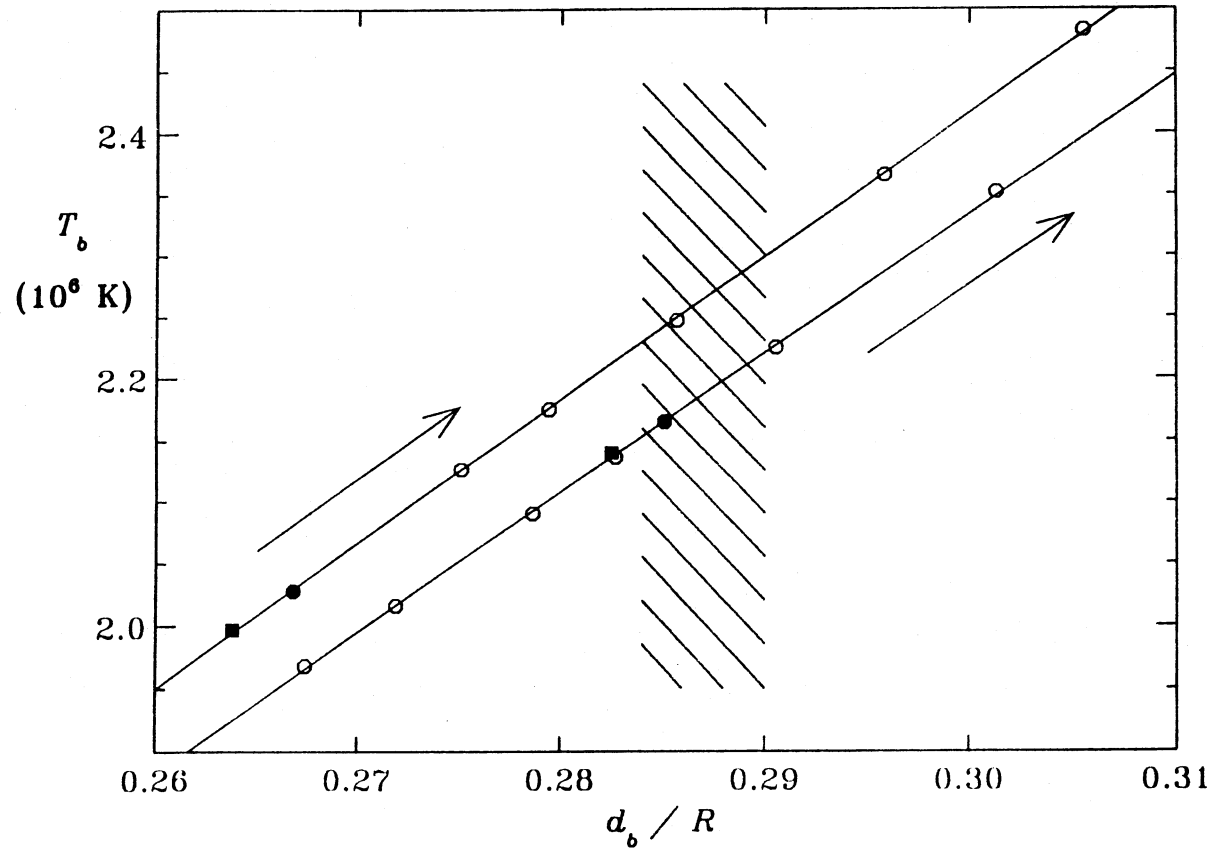

Fig. 11